

USE OF METAL-OXIDE ELECTROCATALYSTS TO CONTROL NOx EMISSIONS FROM FIXED SOURCES

M.A. PETRIK

HELIPUMP CORPORATION
8435 BRECKSVILLE RD
CLEVELAND OH 44141

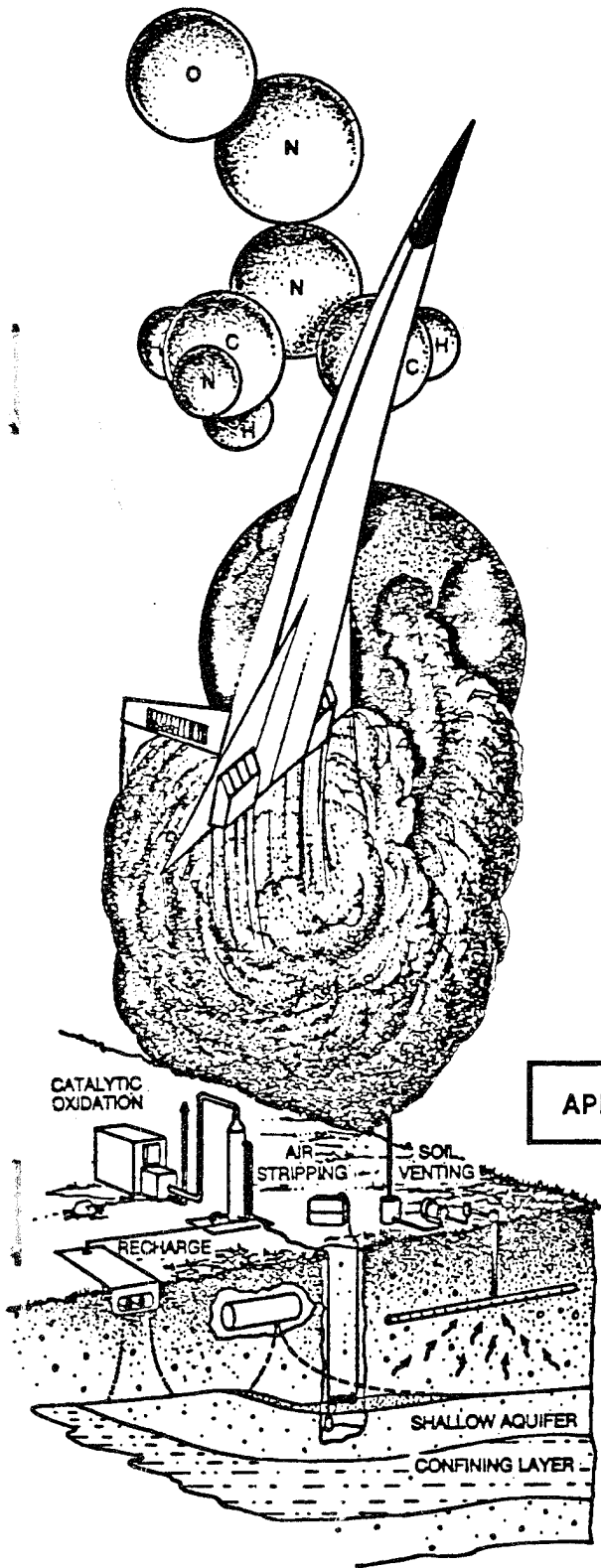
SEPTEMBER 1990

FINAL REPORT

NOVEMBER 1988 — MAY 1989

DTIC QUALITY INSPECTED 3

APPROVED FOR PUBLIC RELEASE: DISTRIBUTION UNLIMITED



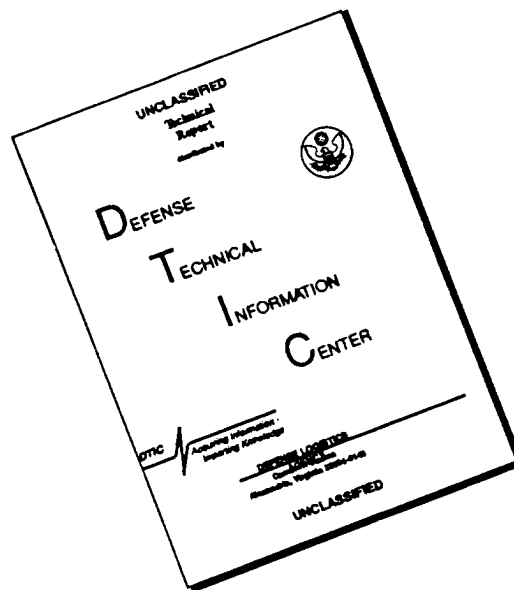
19960619 065



ENVIRONICS DIVISION
Air Force Engineering & Services Center
ENGINEERING & SERVICES LABORATORY
Tyndall Air Force Base, Florida 32403



DISCLAIMER NOTICE



THIS DOCUMENT IS BEST QUALITY AVAILABLE. THE COPY FURNISHED TO DTIC CONTAINED A SIGNIFICANT NUMBER OF PAGES WHICH DO NOT REPRODUCE LEGIBLY.

NOTICE

PLEASE DO NOT REQUEST COPIES OF THIS REPORT FROM
HQ AFESC/RD (ENGINEERING AND SERVICES LABORATORY).
ADDITIONAL COPIES MAY BE PURCHASED FROM:

NATIONAL TECHNICAL INFORMATION SERVICE
5285 PORT ROYAL ROAD
SPRINGFIELD, VIRGINIA 22161

FEDERAL GOVERNMENT AGENCIES AND THEIR CONTRACTORS
REGISTERED WITH DEFENSE TECHNICAL INFORMATION CENTER
SHOULD DIRECT REQUESTS FOR COPIES OF THIS REPORT TO:

DEFENSE TECHNICAL INFORMATION CENTER
CAMERON STATION
ALEXANDRIA, VIRGINIA 22314

REPORT DOCUMENTATION PAGE

Form Approved
OMB No. 0704-0188

1a. REPORT SECURITY CLASSIFICATION UNCLASSIFIED			1b. RESTRICTIVE MARKINGS N/A	
2a. SECURITY CLASSIFICATION AUTHORITY N/A			3. DISTRIBUTION/AVAILABILITY OF REPORT Approved for Public Release Distribution Unlimited	
2b. DECLASSIFICATION/DOWNGRADING SCHEDULE N/A				
4. PERFORMING ORGANIZATION REPORT NUMBER(S) N/A			5. MONITORING ORGANIZATION REPORT NUMBER(S) ESL-TR-89-29	
6a. NAME OF PERFORMING ORGANIZATION Helipump Corporation		6b. OFFICE SYMBOL (if applicable)	7a. NAME OF MONITORING ORGANIZATION Air Force Engineering & Services Center	
6c. ADDRESS (City, State, and ZIP Code) 8435 Brecksville Rd Cleveland OH 44141			7b. ADDRESS (City, State, and ZIP Code) HQ AFESC/RDVS Tyndall AFB FL 32403-6001	
8a. NAME OF FUNDING/SPONSORING ORGANIZATION Engineering & Services Center		8b. OFFICE SYMBOL (if applicable) RDVS	9. PROCUREMENT INSTRUMENT IDENTIFICATION NUMBER F-08635-89-C-0062	
8c. ADDRESS (City, State, and ZIP Code) Air Force Engineering & Services Center Tyndall AFB FL 32403-6001			10. SOURCE OF FUNDING NUMBERS	
			PROGRAM ELEMENT NO. 65502F	PROJECT NO. 3035
11. TITLE (Include Security Classification) Use of Metal-Oxide Electrocatalysts to Control NO_x Emissions from Fixed Sources				
12. PERSONAL AUTHOR(S) Michael A. Petrik				
13a. TYPE OF REPORT Final		13b. TIME COVERED FROM 8811 TO 8905	14. DATE OF REPORT (Year, Month, Day) September 1990	15. PAGE COUNT 51
16. SUPPLEMENTARY NOTATION Availability of this report is specified on reverse of the front cover				
17. COSATI CODES			18. SUBJECT TERMS (Continue on reverse if necessary and identify by block number) Nitric Oxide, NO_x, Electrocatalyst, Air Pollution Metal Oxide, Jet Engine Test Cell, Fixed Source	
FIELD	GROUP	SUB-GROUP		
19. ABSTRACT (Continue on reverse if necessary and identify by block number) The objective of this effort was to determine the feasibility of using solid-state electrochemical technology to remove NO_x from the exhaust of jet engines during static firing tests in jet engine test cells. This report details laboratory testing of electrolytes and spread-sheet-based design calculations. Data and design calculations suggest that electrochemical control of NO_x is feasible in challenging environments; however, implementation of a practical solid-state electrochemical NO_x emission control device will require advances in the state of the art of electrocatalyst preparation that increase selectivity toward nitric oxide (NO) versus oxygen.				
20. DISTRIBUTION/AVAILABILITY OF ABSTRACT <input type="checkbox"/> UNCLASSIFIED/UNLIMITED <input type="checkbox"/> SAME AS RPT. <input type="checkbox"/> DTIC USERS			21. ABSTRACT SECURITY CLASSIFICATION UNCLASSIFIED	
22a. NAME OF RESPONSIBLE INDIVIDUAL Joseph D. Wander			22b. TELEPHONE (Include Area Code) 904 283-4234	22c. OFFICE SYMBOL HQ AFESC/RDVS

EXECUTIVE SUMMARY

Use of Metal-Oxide Electrocatalysts to Control NOx Emissions from Fixed Sources

OBJECTIVE: The objective of this project was to determine the effectiveness of surface-coated conducting ceramics as electrocatalysts for the conversion of nitric oxide (NO) into nitrogen and oxygen.

BACKGROUND: Polluting byproducts of combustion in jet engines are subject to regulation as fixed sources during static firing tests in jet engine test cells (JETCs). In a combat environment, the same emissions have significance as an observable signature, and design improvements will evolve to minimize these signatures. The design modifications will incidentally decrease the environmental moment of the engine operation, including static testing. However, inventories of engines turn over only after 10-20 years in service, so postgeneration treatment of JETC emissions to remove soot particles and NOx will be needed for at least 20 years until the current generation of engines is retired.

The present standard for flue gas treatment is selective catalytic reduction (SCR). SCR requires close control of process temperature and introduces a hazardous substance (ammonia) as part of the process. If temperature control or flow rates drift, SCR is at risk for emitting pollutants. The present study was undertaken in search of a technology that is at least as efficient as SCR at removing NOx, but that is more tolerant of variations of conditions and avoids the use of hazardous reagents.

SCOPE: This project was a Phase I Small Business Innovative Research (SBIR) program in which yttria-stabilized zirconia or ceria was coated with compounds of iron, vanadium, molybdenum, tungsten, nickel, or a proprietary group VIII metal; these catalysts were fired at a temperature between 700 and 1600°C prior to use. Evaluation of their capacity to reduce NOx was surveyed as a function of metal coating, firing temperature, percent oxygen present and reaction temperature.

METHODOLOGY: NO concentration was measured in the gas stream before and after exposure to an electrocatalyst (EC); these measurements were effectively continuous, so averaging over time gave reliable values. This approach directly addresses the question of NO removal. Variations in temperature are needed because JETC operation occurs over a range of temperatures during each firing cycle. Oxygen content began at none and was increased to only several percent because the present catalysts exhibit little or no selectivity for NO over oxygen, and a few percent oxygen in the stream strongly inhibits them. Firing temperatures were varied to obtain empirical information about the sensitivity of these catalysts to conditions of preparation and operation.

TEST DESCRIPTION: Each test consisted of mounting a ceramic electrolyte, coated with the catalyst to be tested, in a quartz tube, flowing pure nitrogen through the tube until all measurable traces of oxygen had been removed, switching the flowing gas to a mixture of 500 ppm NO (20 - 100 cm³/min) in nitrogen, and applying a potential of 0-1.5 V to the catalyst-coated electrolyte. Measurements were made of the concentration of NO downstream of the catalyst and of the current drawn by the catalyst-coated electrolyte. The gas stream was then switched again to introduce 0.3-8 percent oxygen (at the same net flow rate), and the measurements of NO and current were repeated.

RESULTS: Whereas fair (as much as 50 percent) reduction of NO was observed at residence times of the order of seconds in the absence of oxygen, a few percent oxygen (significantly less than encountered in JETC operation) destroyed the efficiency of reduction of NO by these catalysts.

CONCLUSIONS: At their present state of development, electrocatalysts are of no value in controlling NO_x emissions in the oxygen-rich environments typical of JETCs; however, the principle is sound, and an increase by about an order of magnitude in the selectivity of these catalysts for NO in the presence of oxygen should be sufficient to permit their use in such environments.

RECOMMENDATION: Wait for or support continued development of ceramic-based ECs. Reexamine ceramic-based ECs again for this application when state of the art has advanced.

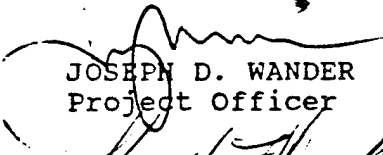
PREFACE

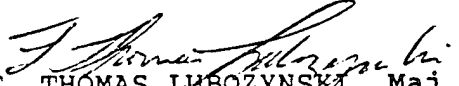
This report was prepared by Helipump Corporation, 8435 Brecksville Road, Cleveland, Ohio 44141, under contract F08635-89-C-0062, for the Air Force Engineering and Services Center, Engineering and Services Laboratory, Tyndall Air Force Base, Florida.

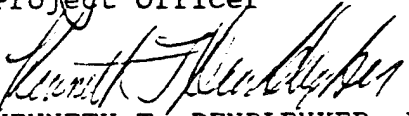
This technical report summarizes work done between 30 November 1988 and 30 May 1989. It was submitted as part of the Small Business Innovative Research (SBIR) Program and has been published, according to SBIR directives, in the format in which it was submitted. Dr. Joseph D. Wander was the AFESC/RDVS project officer.

This report has been reviewed by the Public Affairs Officer (PA), and it may be released to the National Technical Information Service (NTIS). At NTIS, this document will be available to the general public, including foreign nationals.

This technical report has been reviewed and is approved for publication.


JOSEPH D. WANDER
Project Officer


F. THOMAS LUBOZYNSKI, Maj, USAF, BSC
Chief, Environics Division


KENNETH T. DENBLEYKER, Maj, USAF
Chief, Environmental Sciences
Branch



FRANK P. GALLAGHER III, Col, USAF, BSC
Director, Engineering and Services
Laboratory

TABLE OF CONTENTS

Section	Title	Page
I	INTRODUCTION.....	1
	A. OBJECTIVE.....	1
	B. BACKGROUND.....	1
	1. NOx Production Mechanisms and Thermodynamics.....	1
	2. Electrode and Overall Process Reactions.....	2
	3. Electrical Measurements and NOx Removal Rates.....	4
	4. Selective Electrochemical Reduction.	4
	C. SCOPE.....	6
	1. Electrochemical Issues.....	6
	2. Materials.....	7
	3. Engineering.....	7
II	EXPERIMENTS AND RESULTS.....	9
	A. EQUIPMENT.....	9
	1. Low-Temperature Disk Reactor.....	9
	2. High-Temperature Disk Reactor.....	9
	3. High-Temperature Honeycomb Reactor..	14
	4. Low-Temperature Plate Reactors.....	14
	B. EXPERIMENTAL DESIGN.....	20
	C. EXPERIMENTAL RESULTS.....	23
	1. Low-Temperature Runs.....	23
	2. High-Temperature Runs.....	27
	D. SPREAD SHEET ANALYSIS.....	27
	1. Assumptions.....	27
	2. Equations.....	31
	a. Pressure Drop.....	31
	b. Minimum Electrolyte Surface Area.....	32
	c. Actual Width and Height of Reactor and Equivalent Diameter.....	33
	3. Results.....	33
	E. PRELIMINARY SIZING AND ECONOMICS.....	39
III	CONCLUSIONS AND RECOMMENDATIONS.....	40
	A. CONCLUSIONS.....	40
	B. RECOMMENDATIONS.....	40
	REFERENCES.....	41

LIST OF FIGURES

Figure	Title	Page
1	Molecular Scale Schematic.....	3
2	Standard Reduction Potentials.....	5
3	Quartz Reactor Disk Carrier.....	10
4	Quartz Disk.....	11
5	Tapered Male Connection.....	12
6	Outer Female Quartz Unit.....	13
7	High-Temperature Disk Reactor.....	15
8	Honeycomb Reactor Schematic.....	16
9	Ceramic Electrolyte Holder.....	17
10	Ceramic Reactor Top.....	18
11	Ceramic Tube.....	19
12	Outer Cylinder Sleeve Assembly.....	21
13	Inner Reactor Assembly.....	22
14	Time Profile of NO Decomposition on Solid Electrolyte.....	25
15	Schematic of Test Cell 8.....	30
16	Honeycomb Channel Diagram.....	34

LIST OF TABLES

Table	Title	Page
1	NO REMOVAL TESTS WITH ENHANCED-SURFACE-AREA ELECTROLYTES.....	24
2	NO REMOVAL TESTS WITH ELECTROCATALYSTS AND ENHANCED-SURFACE-AREA ELECTROLYTES.....	24
3	SELECTIVITY TESTS - NO REMOVAL TESTS WITH ELECTROCATALYSTS AND ENHANCED SURFACE AREA ELECTROLYTES IN THE PRESENCE OF OXYGEN.....	26
4	NO REDUCTION ACTIVITY - NO REDUCTION TESTS USING HIGH-TEMPERATURE DISKS IN THE ABSENCE OF OXYGEN.....	28
5	HIGH-TEMPERATURE DISK RUNS - NO REMOVAL TESTS WITH ELECTROCATALYSTS IN THE ABSENCE OF OXYGEN.....	28
6	HIGH-TEMPERATURE HONEYCOMB RUNS - NO REMOVAL TESTS WITH ELECTROCATALYSTS IN THE PRESENCE OF OXYGEN.....	29
7	EFFECT OF CHANGES IN HONEYCOMB CHANNEL SIZE..	36
8	EFFECT OF CHANGES IN HONEYCOMB CHANNEL SIZE (8-FOOT WIDE REACTOR).....	36
9	EFFECT OF CHANGES IN REACTOR LENGTH ON 500° C REACTOR.....	37
10	EFFECT OF CHANGES IN NUMBER OF CELLS AND REACTOR WIDTH ON 1000° C REACTOR.....	37
11	EFFECT OF CHANGES IN REACTOR LENGTH ON PRESSURE DROP IN 1000° C REACTOR.....	38
12	EFFECT OF CHANGES IN CURRENT EFFICIENCY ON MINIMUM ELECTROLYTE SURFACE AREA IN 1000° C REACTOR.....	38

LIST OF ABBREVIATIONS

DOE	Department of Energy
EGT	Exhaust Gas Treatment
GRI	Gas Research Institute
METC	Morgantown Energy Technology Center
NDIR	Non-Dispersive Infrared
NOx	Nitrogen Oxides
PETC	Pittsburgh Energy Technology Center
Re	Reynolds Number
SCe	Stabilized Ceria
SCR	Selective Catalytic Reduction
SZ	Stabilized Zirconia
YSZ	Yttria-Stabilized Zirconia

SECTION I

INTRODUCTION

A. OBJECTIVE

The primary goal of the research was to determine the feasibility of using solid-state, electrochemical technology for the removal of nitrogen oxides (NOx) from jet engine test cell exhaust gases. Laboratory-scale experiments provided data for preliminary, computer-based, system designs that conform to pressure drop and size constraints.

B. BACKGROUND

Nitrogen oxides (NOx) formed in the high temperature combustion zone of military incinerators and jet engine processes pose both environmental and health hazards. The acid and toxic properties of NOx have brought about government regulations to reduce or eliminate NOx emissions to the atmosphere. Combustion modification methods to reduce NOx emissions are not acceptable for military jet engine applications. Thus, postcombustion exhaust gas treatment (EGT), such as solid-state electrocatalytic NOx reduction, is required.

Presently the best available EGT technology is the ammonia-based selective catalytic reduction (SCR). In SCR, ammonia is injected into the exhaust gas, and reacts catalytically with NOx to produce elemental nitrogen and water. SCR is sensitive to changes in temperature, exhaust gas flow rate, NOx concentration, and engine load variations. Care must be taken to avoid blow-by of ammonia past the catalyst. Under favorable conditions SCR is capable of reducing NOx emissions by up to 80-95 percent. (Reference 1)

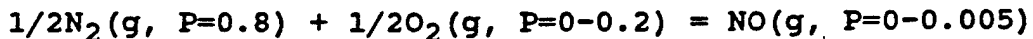
The proposed NOx emissions control technology is a post-combustion EGT based on a solid-state, electrochemical cell. There are no moving parts or consumables; nitrogen and oxygen are the only products. The electrolyte is a high-surface-area solid ceramic oxide ion conductor such as stabilized zirconia (SZ) or stabilized ceria (SCe). The electrodes may be any electronically conductive stable material; previous laboratory tests were performed using porous, high-surface-area silver.

Preliminary Feasibility Study experiments demonstrated the feasibility of using the solid-state electrochemical NOx emission control technology to remove NOx from natural-gas-fired prime movers and defined the problems that must be addressed to assure commercial viability. (Reference 2)

1. NOx Production Mechanisms and Thermodynamics

Combustion of fuels produces NOx principally from the direct, high-temperature reaction of oxygen and nitrogen contained

in the combustion air. This thermally driven fixation of nitrogen is described by the following chemical equation:



where all of the species are gases and the pressures are given in atmospheres. The partial pressure of oxygen is an adjustable combustion parameter, and the maximum equilibrium partial pressure of nitric oxide in a natural gas flame is roughly 5000 ppm (0.5v%).

The thermodynamic equilibrium constant for this chemical reaction (fuel lean conditions) is (Reference 3):

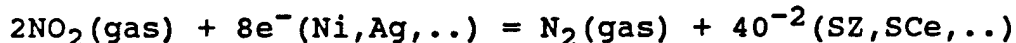
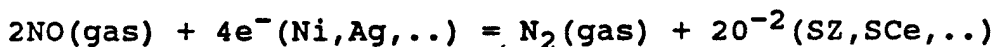
$$K_{eq} = [NO]/[N_2]^{1/2}[O_2]^{1/2} = 4.69 \exp(-21,600/RT)$$

where K_{eq} is the thermodynamic equilibrium constant for thermal nitrogen fixation, R is the universal gas constant, T is the absolute temperature, and $[XX]$ is the concentration, partial pressure, or mole fraction of the gaseous reactants and product, expressed in consistent units.

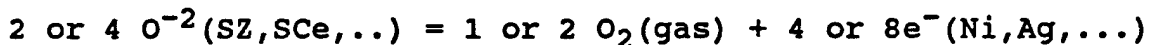
2. Electrode and Overall Process Reactions

As the NO_x-containing exhaust gas passes through the cell, it contacts the high-surface-area, solid electrolyte. In the cathodic zone of the cell, electrochemical reduction takes place, yielding nitrogen gas and oxygen ions. The nitrogen is swept along by the exhaust gas while the oxygen ions dissolve in the solid electrolyte. Simultaneously, in the anodic zone, an equivalent number of oxide ions are converted into oxygen gas and released into the exhaust gas stream.

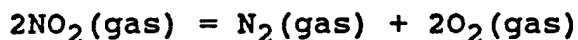
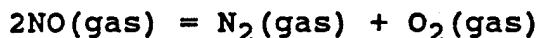
The cathodic electrode reactions are:



The anodic electrode reaction is:



The overall process is:



A molecular-scale schematic believed to represent the cathodic electrode reaction process is shown in Figure 1. The nitric oxide molecule reacts at the three-phase boundary electrode-electrolyte-exhaust gas; N₂ gas is swept away by the exhaust gas and oxygen ions (O²⁻) dissolve in the solid electrolyte.

Because oxygen is also removed at the electrolyte three-phase boundary, the exhaust from the jet engines poses a special problem. To minimize parasitic power losses caused by the removal of oxygen in competition with NO, the solid electrolyte must be made selective to NO over oxygen.

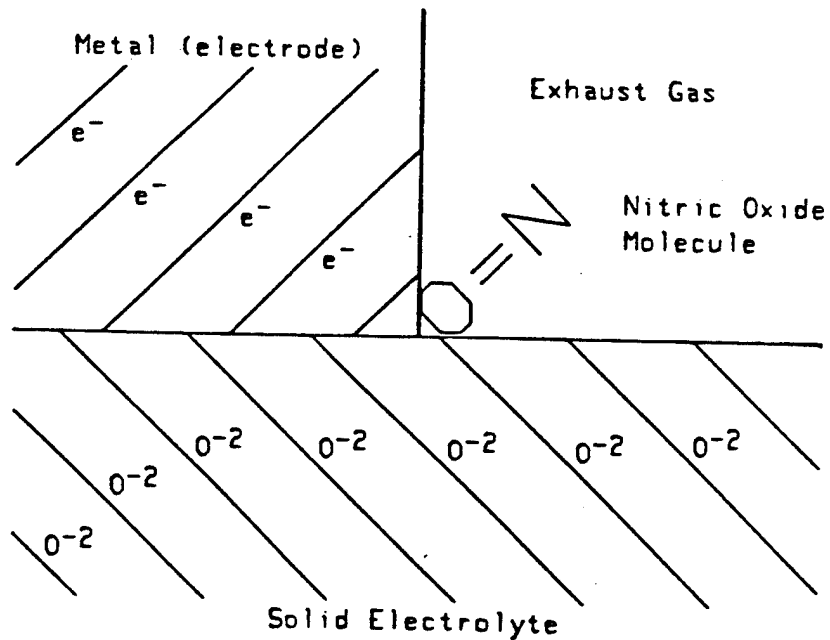


Figure 1. Molecular Scale Schematic

3. Electrical Measurements and NOx Removal Rates

The relationship between the current passing through the reactor and the removal of NOx is as follows:

$$\begin{aligned}i &= i_{\text{ionic}} + i_{\text{electronic}} \\ &= i_{\text{ionic}} + i_e\end{aligned}$$

The observed current is the sum of two discrete currents. The ionic current is associated with the transport of oxide ions and the removal of NOx, while the electronic current is a background noise caused by impurities and defects in the electrolyte. The useful ionic current may therefore be defined as:

$$i - i_e = i_{\text{ionic}}$$

The value of i_{ionic} may be related to the rate and efficiency of NOx removal according to Faraday's Law:

$$i_{\text{ionic}} = (F) (N_{\text{eq}}) (\text{gram-moles NOx removed/second})$$

where

F = Faraday's constant, 96,489 Coulomb/equivalent
 N_{eq} = number of electrons transferred per molecule of NOx reacted; 2 for NO, 4 for NO₂, and in general 2 for each oxygen atom participating in the reaction.

One amp of ionic current corresponds to an NO decomposition rate of 9.3 milligrams per minute (if NO is the only source of oxygen). NO decomposition rate will be diminished by the presence of oxygen if NO is not selectively removed over oxygen. Through an equation of state, the ionic current may also be expressed as a function of gas flow rate and the change in NOx concentration across the reactor; the ideal gas law is adequate at the high-temperature, low-pressure conditions of the reactor.

$$i_{\text{ionic}} = (F) (P) (N_{\text{eq}}) (V) (Y_{\text{NOx}}) / RT$$

where

V = volumetric gas flow rate measured at T,P; T,P need not be at reactor operating conditions
P = pressure
T = absolute temperature
R = universal gas constant
 Y_{NOx} = change in NOx mole fraction across reactor

4. Selective Electrochemical Reduction

Exhaust gases contain a number of compounds that may, in principle, be reduced (or oxidized) within the reactor. In general, only NOx is intended to be reduced. Additional exhaust gas

reactions, such as the reduction of water, are undesirable, power-consuming side reactions.

The standard potentials of several possible electrochemical reactions are displayed in Figure 2 (Reference 4). Chemical reactions that occur spontaneously have a negative Gibbs' energy and a positive standard potential. All of the reductions listed in Figure 2, except for the nitrogen fixations, have negative voltages. The oxides NO₂ and NO are thermodynamically unstable and, therefore, have positive voltages.

For the proposed solid-state electrochemical technology to reduce a compound, a potential greater than the thermodynamic potential for that compound must be applied across the reactor. To remove the fundamentally unstable nitrogen oxides, any cathodic voltage will suffice. However, to reduce the more thermodynamically stable species such as CO₂ or H₂O, a potential greater than about 1 volt must be applied. Thus, NO_x may be selectively removed from an exhaust gas stream by maintaining the applied potential below that required to reduce the nonpolluting species - roughly 1 volt for exhaust gases below about 1000°C (boilers, engines, vehicles, etc.).

NO_x selectivity is measured in the current efficiency of the cell. The current efficiency is the ratio of current theoretically required to reduce NO_x to total current applied. The NO_x reduction current can be calculated from analytical data, the flow rate to the reactor (to calculate gmoles NO_x/sec reduced) and Faraday's Law.

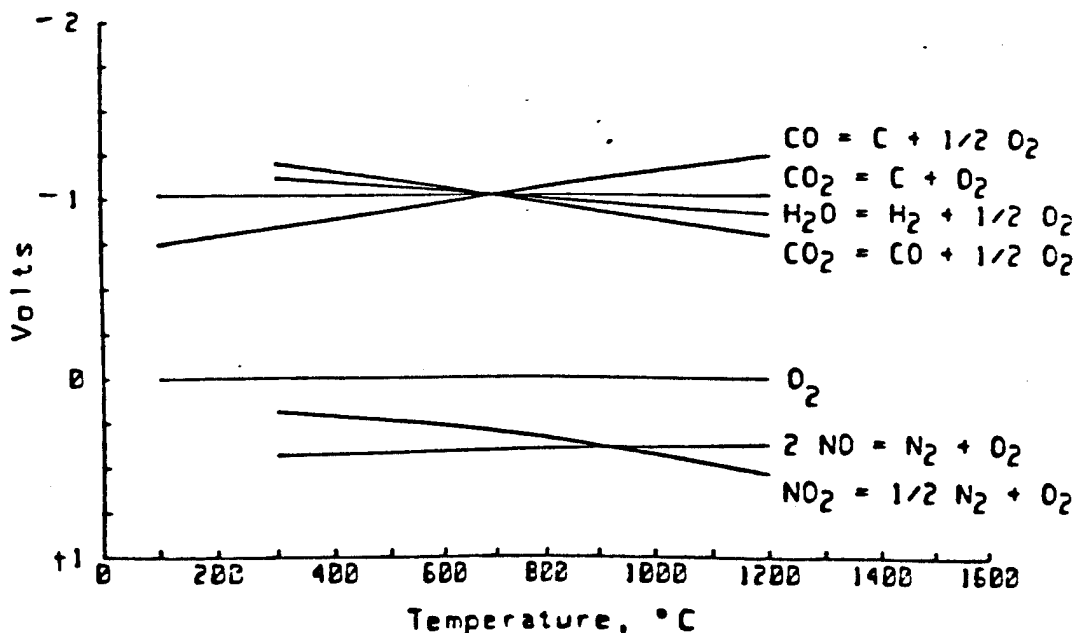


Figure 2. Standard Reduction Potentials

C. SCOPE

Preliminary studies identified several technical problems that require further attention to achieve proof-of-concept and scale-up to commercial size. The technical problems fall into three general categories: (1) Electrochemical, (2) Materials, and (3) Engineering. The goal of the Phase I work was to design an electrochemical NO_x emission control reactor that could selectively remove NO_x emissions from jet engine test cells within the size and pressure-drop constraints allowed by these cells. The design would also include preliminary capital and operating costs (in the form of power consumption). Bench-scale tests using existing equipment from other government projects would be used to determine activity of electrolytes in NO_x reduction and selectivity for NO_x over oxygen.

1. Electrochemistry

The solid-state electrochemical NO_x emissions control technology is based on two general concepts, transport of oxygen ions through a ceramic phase, and electrocatalytic reduction of NO_x to nitrogen gas and oxygen ions at the ceramic surface. The ideal reactor would have high NO_x selectivity at the ceramic surface, to adsorb NO_x in preference to oxygen, and high ionic conductivity through the bulk ceramic phase, to minimize electrical power costs.

Bulk ionic conductivity has been found in stabilized cerias and stabilized zirconias. Ionic conductivity is a strong function of the concentration and type of stabilizing agent, and it is also an exponential function of temperature. In general, at process temperatures, cerias are more ionically conductive than zirconias.

Selectivity for NO_x can be enhanced by loading the surface of the electrolyte with certain catalytic agents. The catalytic agents, usually transition metals, strongly and preferentially bind NO in the presence of O₂. Thus the cathodic surface is coated with NO molecules in lieu of oxygen molecules. As only the gas molecules bound to the coated cathodic surface of the electrolyte are reduced, a net selectivity for NO_x over oxygen results. A large number of these catalytic materials are reported in the literature (References 5,6,7,8). For example, NO_x is toxic because iron in hemoglobin preferentially adsorbs nitrogen oxides, even in the presence of an excess of oxygen.

In general, these catalytic agents are based on transition metal compounds selected from the left-hand side of the periodic chart. Attractive NO_x-selective catalytic agents are iron, molybdenum, chromium, vanadium, and tungsten metals and compounds thereof, including such nonoxide materials as nitrides, carbides, borides, or silicides. All of these transition metals are known to bind NO strongly and preferentially, even in the presence of excesses of oxygen (References 5,6,7,8).

The efficiency of the technology for the removal of NO_x can be enhanced by increasing the surface area of the electrolyte. Increasing surface area of the electrolyte provides greater numbers

of electrocatalytically active sites for NOx reduction. The result is lower process operating and capital costs.

The solid-state electrochemical technology requires electronic conductivity (i.e., porous electrodes) at the surface of the ceramic electrolyte to pass current to the cell and to assist in the electrocatalytic reduction of NOx to nitrogen gas and oxygen ions. Although silver functioned as the electrode material in Preliminary Feasibility work, studies to improve and optimize electrode materials are needed. Porous electrode materials that conduct both electrons and oxide ions (mixed conductors), are particularly attractive because they may increase the total number of electrocatalytically active sites.

2. Materials

One objective of the ongoing solid-state, electrochemical NOx emission control technology is to develop a family of scaled-up flow-through ceramic reactor elements that have high surface area, good mechanical properties, good oxygen ion conductivity, and low electronic conductivity at process temperatures.

Physical and mechanical properties are important in the design, fabrication, and operation of a commercially viable technology. Among the important properties to be determined are porosity, physical integrity, and thermal integrity of both the reticulate and the solid ceramic.

Surface modifications of the bulk ceramic may be required to maximize electrocatalytic reduction of NOx and efficient distribution of current to the ceramic surface. These modifications may include doping the surface with electrocatalytic agents, making the surface a mixed ionic and electronic conductor, and maximizing surface area.

Fabrication techniques are determined from information obtained on ceramic composition, physical and mechanical properties, and required surface modifications. Ceramic composition determine what materials should be used in fabrication. Physical and mechanical properties dictate what reactor sizes and shapes can be fabricated, and what physical and thermal stresses can be expected with those shapes and sizes. Surface modification techniques are important in determining some of the fabrication steps and their sequence. Product uniformity, both physical and chemical, will be a major fabrication concern.

3. Engineering

Engineering considerations during all phases of testing, from the electrochemical optimization to prototype geometries to the final demonstration tests, are important to the ultimate commercial success of the technology. Engineering factors appear in the design and fabrication of the ceramic electrolyte and the electrochemical reactor, as well as in all the supporting operational, analytical, and control equipment.

Determination of the optimum material and electrochemical properties permits design of an electrochemical reactor, which can eventually be scaled up for field tests. Physical properties of the ceramics will serve as guidelines for the actual geometry of the cell. Such engineering considerations as sealing requirements, pressure drop, manifolding, insulations, materials of construction, and assembly techniques will also influence the ceramic geometry and the reactor geometry, as will integration of auxiliary equipment such as electrical hookups, heating elements, gas manifolding, blowers, and analytical equipment.

SECTION II

EXPERIMENTS AND RESULTS

A. EQUIPMENT

Experiments were performed using equipment and procedures developed under two Department of Energy (DOE)-sponsored research projects. The first DOE project, through the Pittsburgh Energy Technology Center (PETC), involves the removal of NO_x and SO₂ from coal-fired boiler flue gases. Typically, flue gas exhaust contains approximately 500 ppm NO_x and 1000 ppm SO₂ at 400°C to 500°C, about the same temperature as jet engines near idle. The second DOE project, through Morgantown Energy Technology Center (METC), involves the removal of 400 ppm NO_x and 1500 ppm SO₂ at 1000°C to 1400°C, the lower temperature being approximately equal to a jet engine at full power.

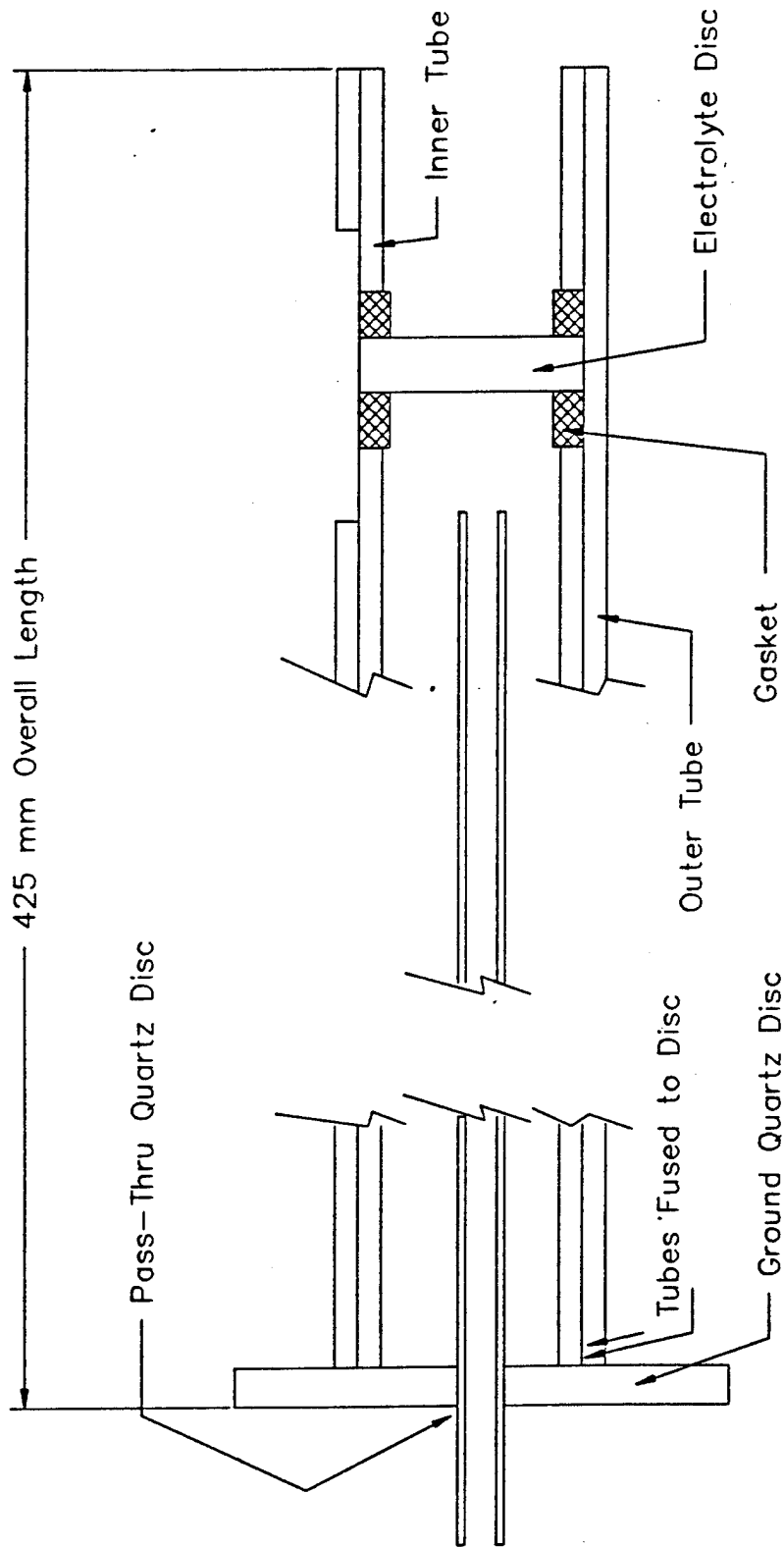
1. Low-Temperature Disk Reactor

Low-temperature experiments were run using the PETC disk reactor. (Reference 9) The reactor is used to test 25-mm diameter, 1- to 2-mm thick ceramic disks for the removal of NO_x in the presence of various gases, usually a combination of nitrogen and oxygen. The system consists of a gas manifold for introducing various gas mixtures into a two-piece quartz reactor located in a temperature-controlled, Lindberg tube furnace. The exhaust gas from the reactor flows to a Horiba Nondispersive Infrared (NDIR) analyzer to determine NO_x concentration.

The quartz reactor is a two-piece device illustrated in Figures 3, 4, 5 and 6. The reactor allows gases to flow into the disk reaction area in the hot zone inside the furnace and allows a seal to be made in the cold zone outside the furnace. Figure 3 shows the inside piece of the reactor which holds the disk. The ceramic disk, along with anode and cathode connecting wires, is held in a slot in the quartz tube by two pieces of heat-expanding gasket material. The test gas flows through the center tube to the cathode side of the disk and back out through the annular region between the center tube and outer tube. The gas passes out through a hole in the quartz disk. Figure 4 shows a detail of the quartz disk. Other holes in the quartz disk are used for electrical connections, thermocouple probe, and anode side gas inflow and outflow. Fused quartz tubes (not shown in Figure 4) are used to make outside connections. The inside reactor piece is sealed to the outside piece with a ground-glass tapered connection (Figure 5, not shown in Figure 3). The male taper fits into the outer piece female taper (Figure 6) to form a gas-tight seal.

2. High-Temperature Disk Reactor

The testing of high-temperature disks was performed in the METC quartz reactor. The reactor system is similar to that used in the low-temperature reactor system with an inlet gas manifold, a controllable tube furnace, the disk reactor, and outlet gas



Quartz Electrode Disc Carrier Assembly	
Designed By: Cook	5/5/1988

Figure 3. Quartz Reactor Disk Carrier

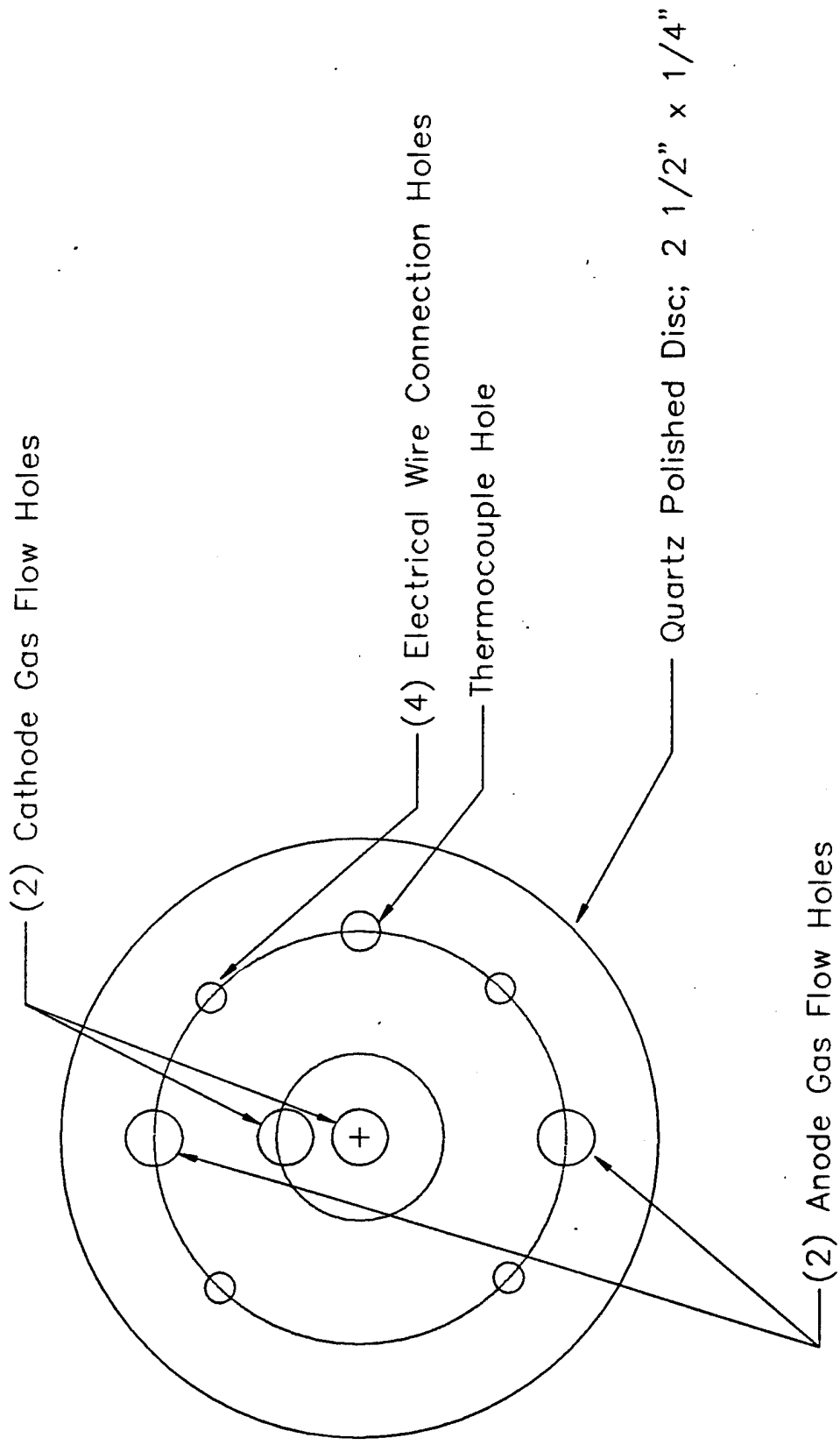


Figure 4. Quartz Disk

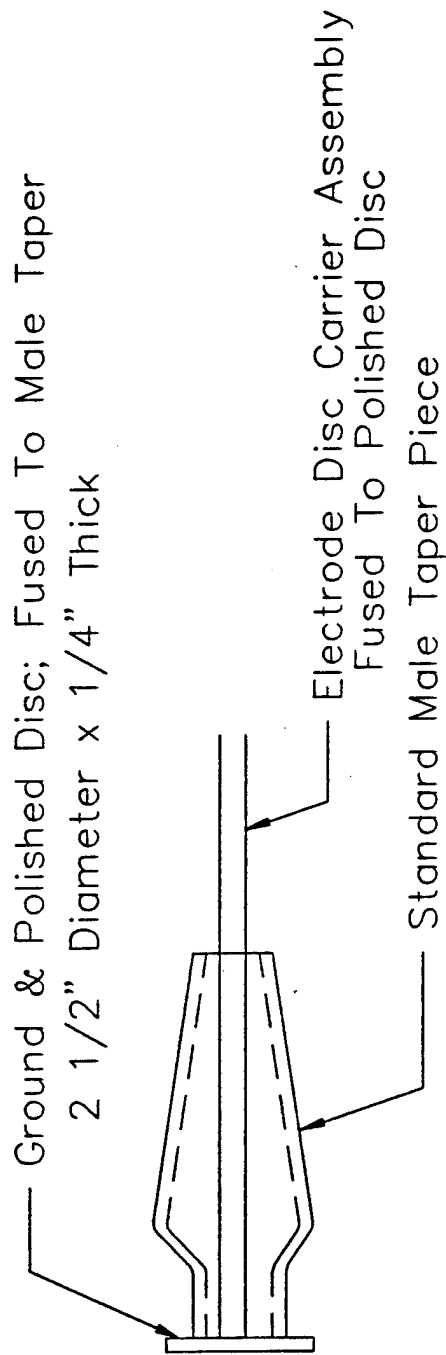



Figure 5. Tapered Male Connection

Female Quartz Unit	
Designed By: Cook	Project: FLU
Measurements in mm.	5/5/1988
 HELIPUMP	

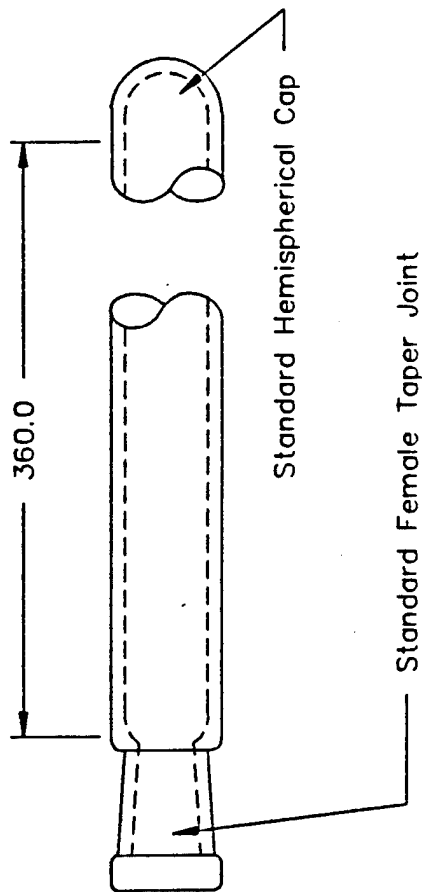


Figure 6. Outer Female Quartz Unit

connection to the NDIR. The reactor is used to test 1.5-inch diameter, 1/16-inch thick, ceramic electrolyte disks at temperatures up to 1400°C.

Figure 7 illustrates the high-temperature disk reactor. The quartz reactor is made up of a small-diameter anode side and larger-diameter cathode side. The disk is placed on the ledge formed between the anodic and cathodic faces. Circular electrode current distributors are held by compression to either side of the disk by a center-entering, quartz tube. The quartz tube is held in place by a Teflon[®] end cap, which seals the cathode section outside the furnace in the cold zone. Ports are available in the Teflon[®] cap for electrical leads and gas flow. A ground glass connection seals the anode side in the cold zone; if desired, gas can be flowed through this connection.

During operation, the test gas flows through the center-entering quartz tube into the reaction sites at the surface of the electrolyte disk in the hot zone of the furnace. The gas then flows through the annular region and out of the reactor through the port in the end cap. The effluent gas is analyzed for NO concentration in the NDIR.

3. High-Temperature Honeycomb Reactor

Figure 8 shows a schematic of the honeycomb reactor. The yttria-stabilized zirconia (YSZ) honeycomb reactor is similar to a conventional automotive catalytic converter. The honeycomb is held in a quartz tube by heat-activated gasket material. When the reactor is heated, the gasket expands, holding the honeycomb in place. The gasket also forces the gas to pass through the reactor and not bypass it. The quartz tubes are sealed in the cold zone with Teflon[®] end caps. Both gas ports and electrical connections are made through the end caps.

4. Low-Temperature Plate Reactors

Two attempts were made to develop low-temperature plate reactors during this project. The reactors were to test 2.5-inch square ceramic electrolyte plates for higher flow rate tests.

The first reactor was constructed from a machinable ceramic material. Figures 9, 10, and 11 show engineering drawings of the reactor. In the reactor, a 2.5-inch square ceramic piece, with electrodes glued to the surface, was placed in the electrolyte holder. Electrical connections were made through the reactor walls and sealed with ceramic glue. An aluminum gasket sealed the electrolyte holder and reactor top. Gas passed through one tube glued into the electrolyte holder, to the electrolyte, and out through another tube. The reactor was heated inside a box furnace. Although a few tests were attempted using this reactor, sealing problems and breakage problems (due to the brittle nature of the machinable ceramic) caused this reactor to be abandoned without obtaining any useful NO_x reduction data.

<table border="1"> <tr><td>□</td><td>□</td><td>□</td><td>□</td></tr> <tr><td>□</td><td>□</td><td>□</td><td>□</td></tr> <tr><td>□</td><td>□</td><td>□</td><td>□</td></tr> <tr><td>□</td><td>□</td><td>□</td><td>□</td></tr> </table>	□	□	□	□	□	□	□	□	□	□	□	□	□	□	□	□	Quartz Reactor Vessel		
□	□	□	□																
□	□	□	□																
□	□	□	□																
□	□	□	□																
<table border="1"> <tr><td>○</td><td>○</td><td>○</td><td>○</td></tr> <tr><td>○</td><td>○</td><td>○</td><td>○</td></tr> <tr><td>○</td><td>○</td><td>○</td><td>○</td></tr> <tr><td>○</td><td>○</td><td>○</td><td>○</td></tr> </table>	○	○	○	○	○	○	○	○	○	○	○	○	○	○	○	○	C:\DWG\FAB\QTZ1	8/3/88	
○	○	○	○																
○	○	○	○																
○	○	○	○																
○	○	○	○																
HELIPUMP	Designed By: L. Siwajek																		
<table border="1"> <tr><td>○</td><td>○</td><td>○</td><td>○</td></tr> <tr><td>○</td><td>○</td><td>○</td><td>○</td></tr> <tr><td>○</td><td>○</td><td>○</td><td>○</td></tr> <tr><td>○</td><td>○</td><td>○</td><td>○</td></tr> </table>	○	○	○	○	○	○	○	○	○	○	○	○	○	○	○	○	All Measurements In MM; Unless Noted Otherwise		
○	○	○	○																
○	○	○	○																
○	○	○	○																
○	○	○	○																

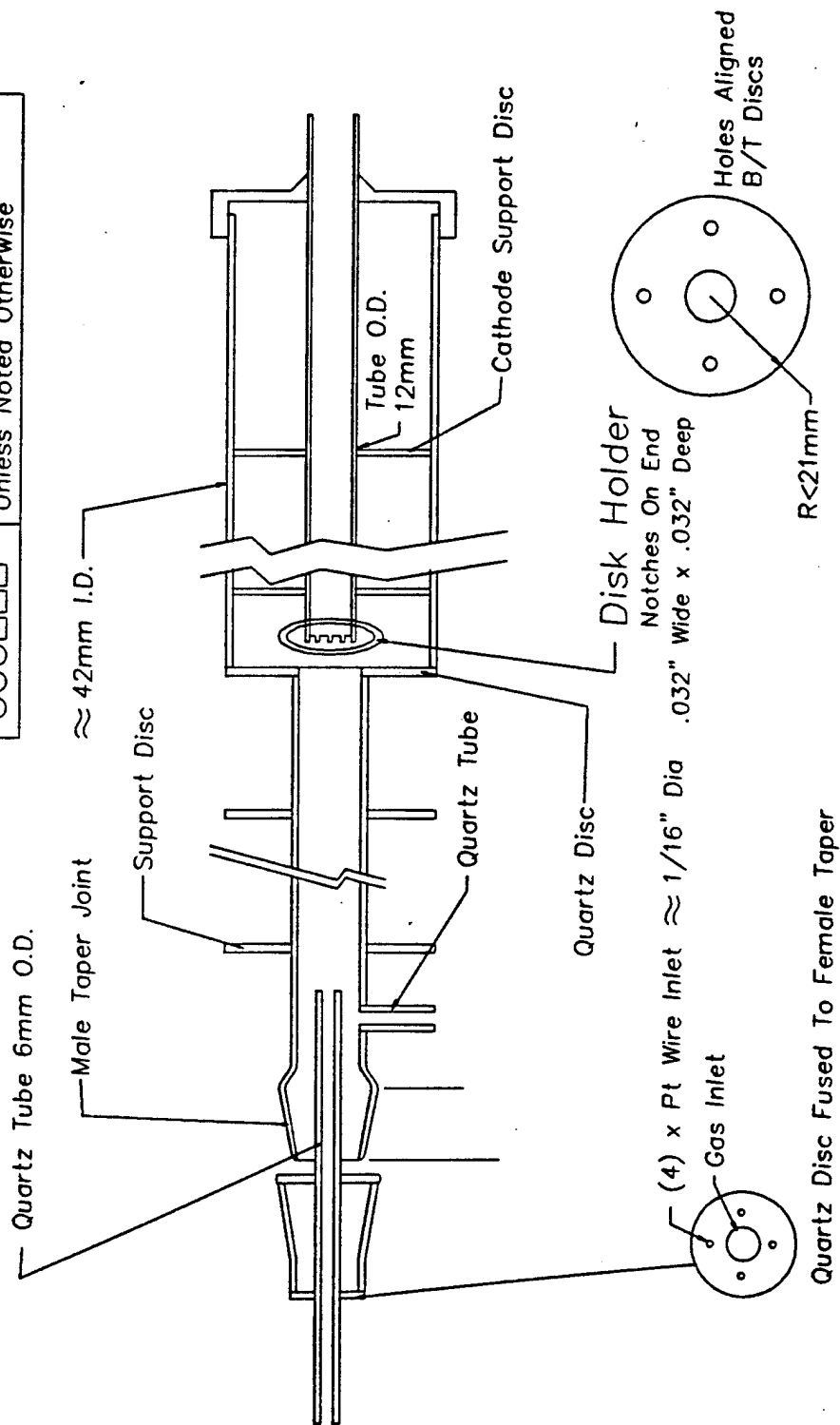


Figure 7. High-Temperature Disk Reactor

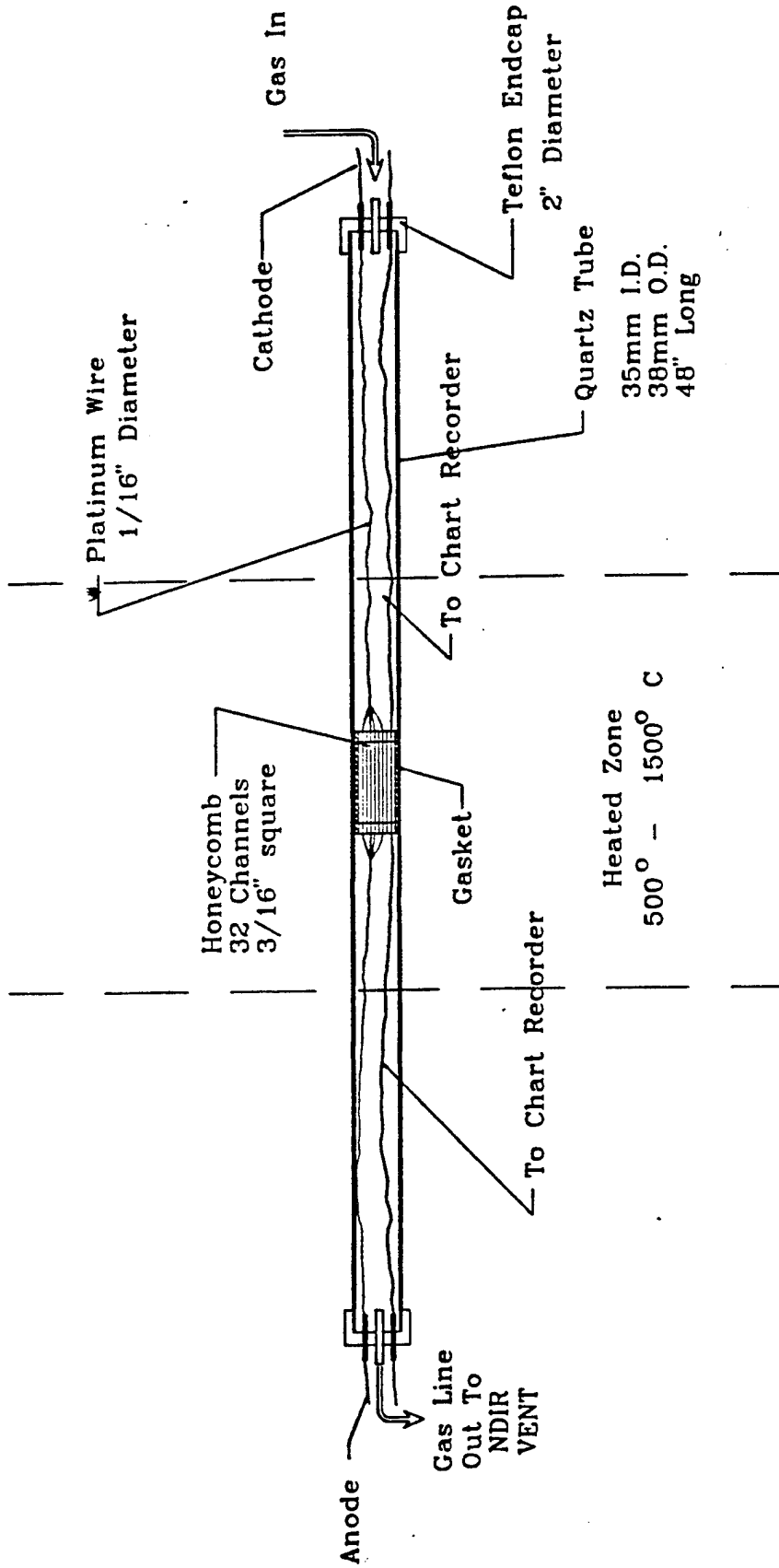
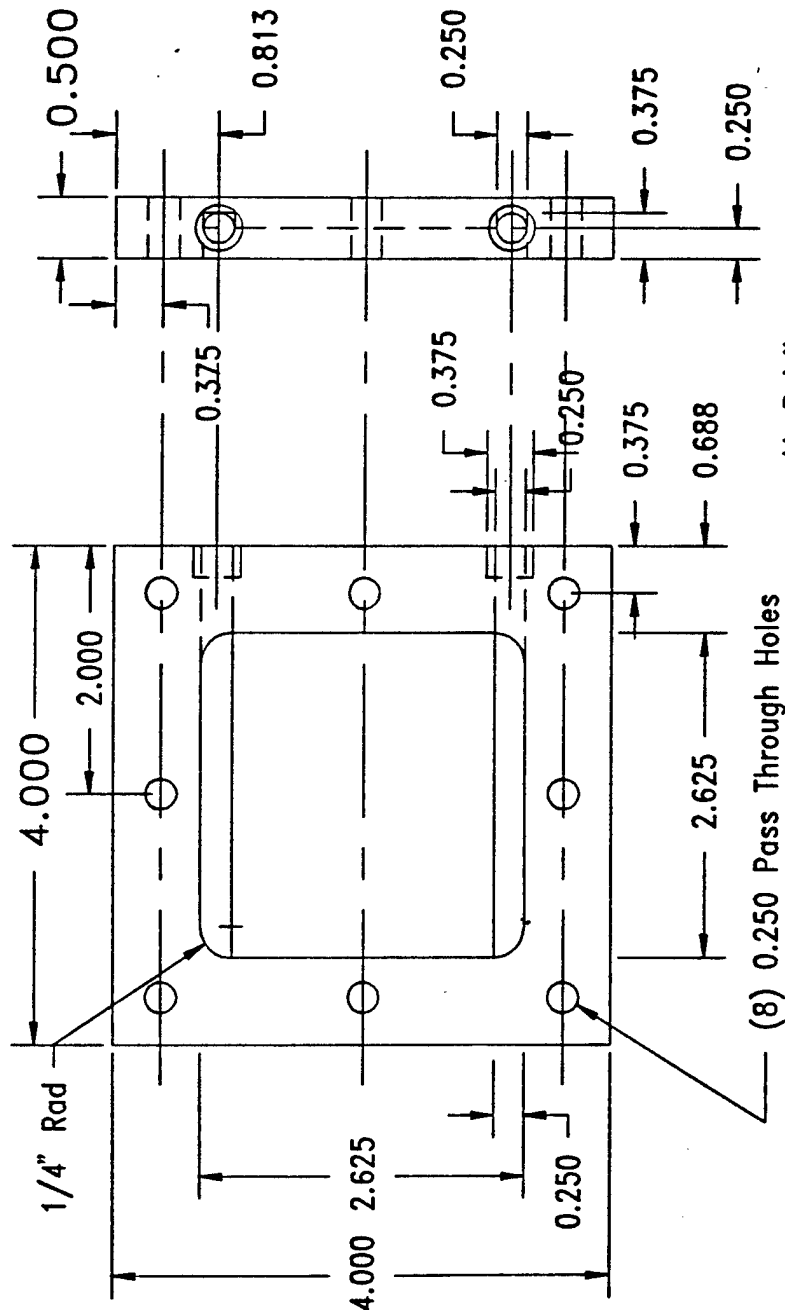


Figure 8. Honeycomb Reactor Schematic

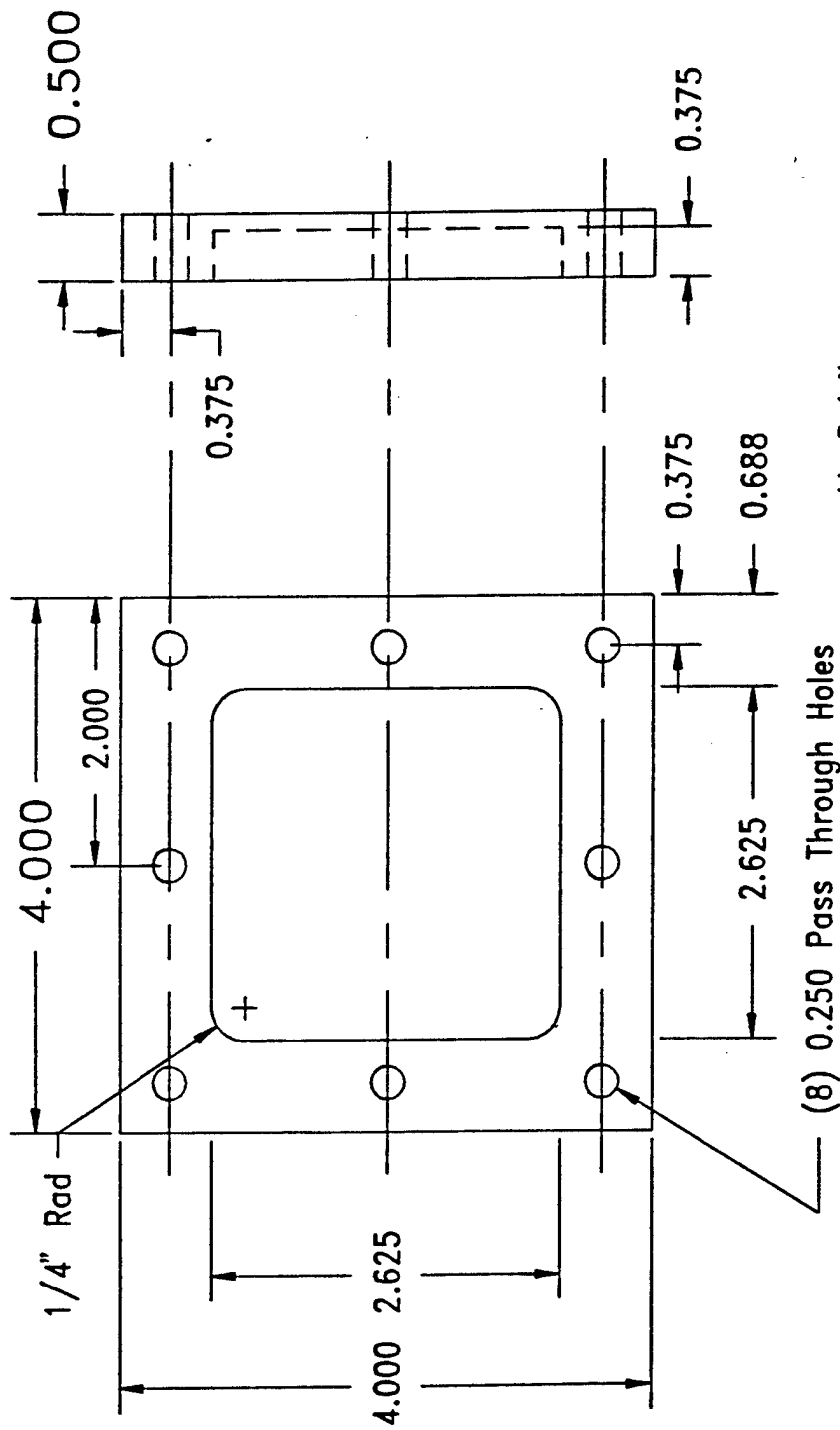


(8) 0.250 Pass Through Holes

M. Petrik
 HELIPUMP CORPORATION
 February 7, 1989

Note: All Tolerances ± 0.005
 Mat'l: Machinable Ceramic
 All Dimensions in inches

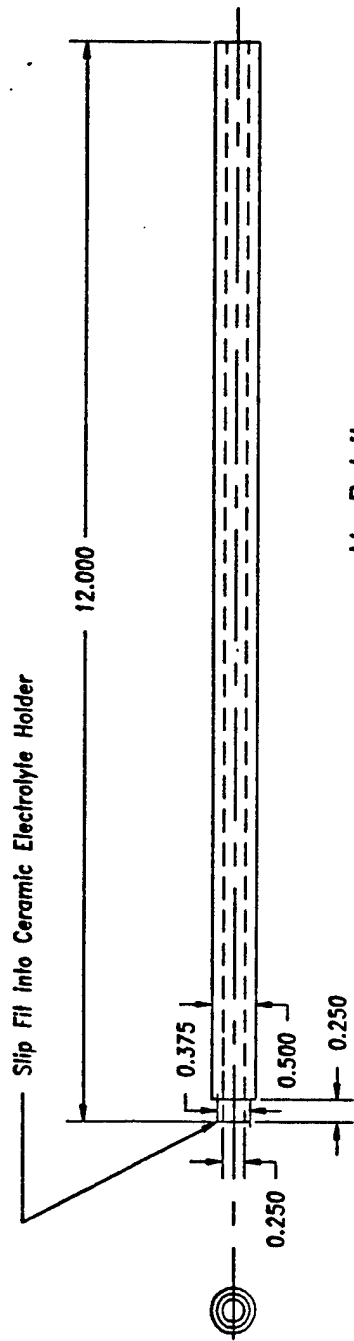
Figure 9. Ceramic Electrolyte Holder



M. Petrik
 HELIPUMP CORPORATION
 February 7, 1989

Note: All Tolerances ± 0.005
 Mat'l: Machinable Ceramic
 All Dimensions in inches

Figure 10. Ceramic Reactor Top



M. Petrik
 HELIPUMP CORPORATION
 February 9, 1989

Note: All Tolerances ± 0.005 unless noted
 Mat'l: Machinable Ceramic
 All Dimensions in Inches

Figure 11. Ceramic Tube

A second reactor was constructed from stainless steel using a design similar to the low-temperature disk reactor. Figures 12 and 13 show assembly drawings of the inner reactor and sleeve assembly. The reactor was constructed from materials available from previous work in our lab. Use of a sleeve-type assembly allowed cold-zone sealing using a standard rubber O-ring. The ceramic electrolyte reactor, with the electrode leads glued on, sat in the end of the inner reactor. Gas to be tested was flowed to the electrolyte by the central tube in the sleeve side of the reactor. The gas flowed around the electrolyte to a central tube on the end of the inner reactor assembly. Initially, the gas was to be heated in a heat exchanger before flowing into the reactor. No sufficiently controllable heating source could be found before the end of this project to test any ceramic plates. Heating sources tested were not able to raise the temperature higher than 250°C.

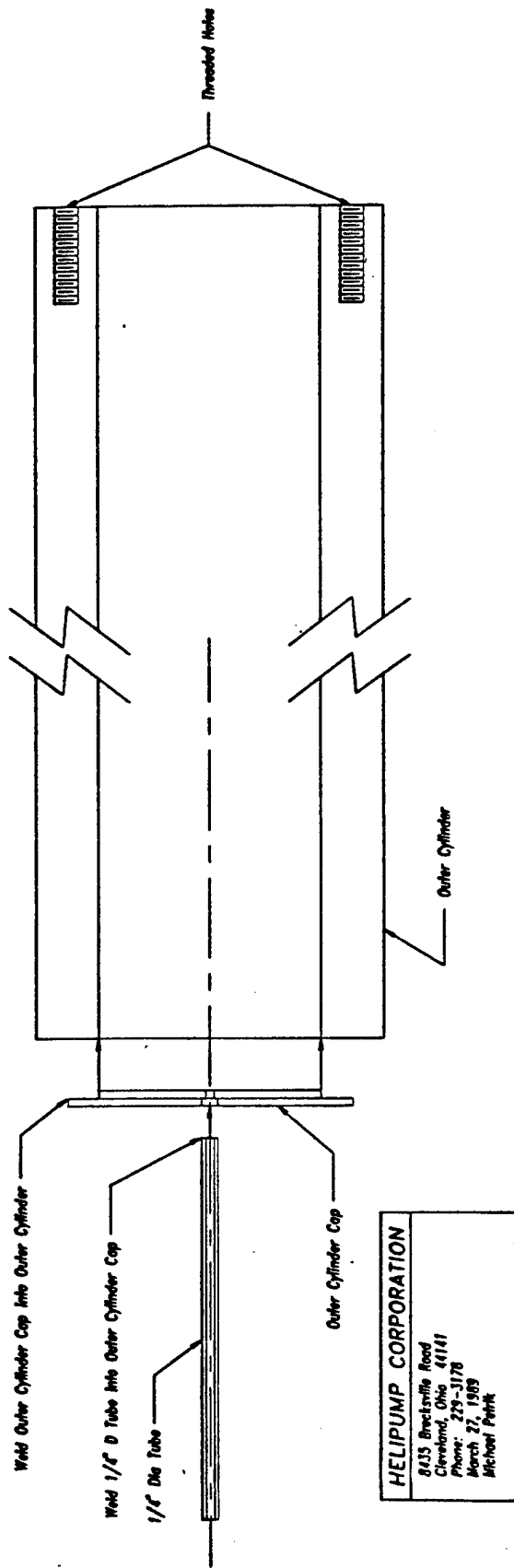
B. EXPERIMENTAL DESIGN

A NO_x emission control technology must be able to remove a large percentage of NO_x from a stream containing a relatively low concentration of NO_x. NO_x removal must also be performed in the presence of various other gases, most importantly oxygen. Experiments were run on various solid electrolyte disks and honeycomb to determine the ability of the solid-state electrochemical system to remove NO_x in both the absence and presence of oxygen. The same testing procedure was used for high-temperature, low-temperature, and honeycomb experiments.

Initial tests with the disks were performed in the absence of oxygen. These tests were used to establish a baseline behavior for a disk and to screen various electrocatalysts for NO_x decomposition activity.

After the electrochemical cell is assembled, nitrogen is flowed through the reactor for several hours to purge the system of oxygen. After purging is complete, the gas is changed to a prepared mixture of 500 ppm NO in nitrogen delivered at a flow rate of 20 to 100 cm³/min. A potential varying from 0 to 1.5 V is applied to the cell. The current is measured for each voltage and the change in NO concentration is measured using the NDIR. The NDIR output is graphically displayed on a Hewlett-Packard model 9836 minicomputer. Plots of NO concentration versus time are output from the computer. Decomposition of NO is confirmed by alternating between the applied voltage and zero voltage.

After current and NO concentration measurements were made, oxygen was introduced to the system. Various concentrations of oxygen (from 0.3 percent to 8 percent) were tested. Total gas flow rate was maintained at the level tested in the absence of oxygen (20 to 100 cm³/min). Various potentials were applied (0 to 1.5 volts) and the current was measured. Changes of NO concentration were measured with the NDIR and graphically output on minicomputer.



HELIPUMP CORPORATION
 8435 Brecksville Road
 Cleveland, Ohio 44141
 Phone: 229-3178
 March 27, 1969
 Michael Peink

Figure 12. Outer Cylinder Sleeve Assembly

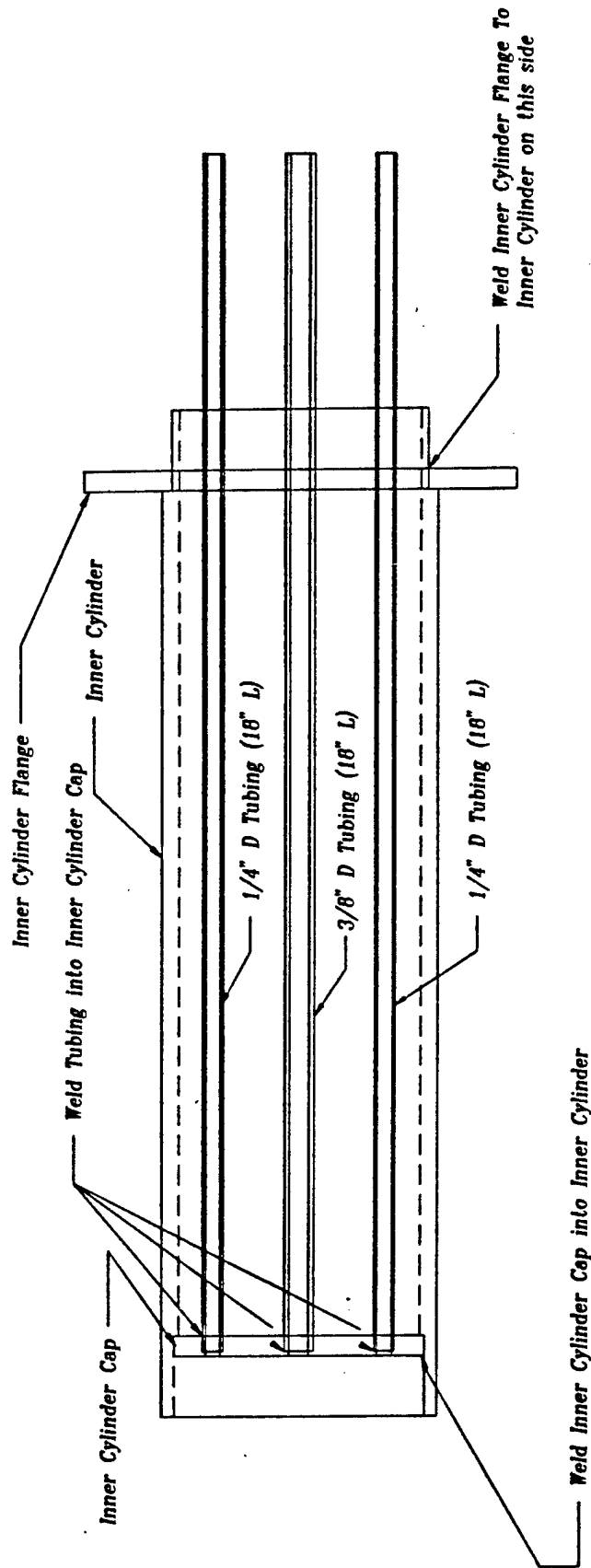


Figure 13. Inner Reactor Assembly

C. EXPERIMENTAL RESULTS

1. Low-Temperature Runs

Low-temperature tests were run with one-inch diameter yttria-stabilized ceria disks supporting various surface area enhancements and electrocatalysts. Preliminary tests were performed to determine the effect of enhanced surface area on NO_x reduction. Surface area enhancement was performed by IGR Enterprises, using proprietary zirconia-base wash coats, sintered at various temperatures. Lower-temperature sintering gave higher surface area coatings due to lower degrees of sintering. Table 1 shows the effect of sintering temperature on NO decomposition from an oxygen-free gas. All tests were run at 500°C at an applied potential of 1.5 VDC.

Table 1 shows that higher-surface-area coatings give higher NO removal. Tests were continued using surface-area-enhanced electrolytes with electrocatalysts. Electrocatalysts were prepared and applied to the electrolyte by IGR Enterprises using proprietary techniques. The electrocatalysts tested were mainly transition metal oxides. Table 2 shows the extent of decomposition of NO by various electrocatalysts having various enhanced surface areas. The proprietary Group 8 transition metal oxide electrocatalyst with the highest surface area (lowest firing temperature) gave 64 percent NO removal and the largest low-temperature current density (22.7 mA/cm²). The proprietary Group 8 transition metal oxide electrocatalyst having the lowest surface area (highest firing temperature) had the highest current efficiency (31.0 percent). By reducing the gas flow rate to 15 cm³/min, equilibrium NO removal up to 80 percent was obtained using the proprietary electrocatalyst (see Figure 14).

The electrocatalysts with enhanced surface area were further tested by adding oxygen to the gas stream. NO_x selectivity over oxygen is indicated by high NO removal percentages at high current efficiencies. The results of NO selectivity tests are shown in Table 3. The results show that, though NO reduction is possible in the absence of oxygen, increasing oxygen in the gas causes NO reduction activity to decrease drastically. The proprietary Group 8 transition metal oxide electrocatalyst showed moderate activity and 5.3 percent current efficiency in the presence of very low oxygen concentrations. Tungsten oxide gave moderate NO reduction in the presence of 2 percent oxygen.

TABLE 1. NO REMOVAL TESTS^a WITH ENHANCED-SURFACE-AREA ELECTROLYTES

Firing Temperature °C	Percent NO Removal
1000	45
1100	28
1300	20
No Enhancement	8 - 25

^a470 ppm NO in N₂; 100 cm³/min flow

TABLE 2. NO REMOVAL TESTS^a WITH ELECTROCATALYSTS AND ENHANCED-SURFACE-AREA ELECTROLYTES

Electrocatalyst Type	Firing Temperature °C	Percentage NO Removal	Current Density mA/cm ²	Current Efficiency %
Proprietary Group 8 Metal Oxide	700	64	22.7	3.8
Proprietary Group 8 Metal Oxide	800	54	6.5	11.0
Proprietary Group 8 Metal Oxide	900	46	2.0	31.0
Iron Oxide	700	30	3.6	11.2
Iron Oxide	800	27	3.4	10.7
Iron Oxide	1000	9	3.0	4.0
Vanadium Oxide	700	15	0.8	25.3
Vanadium Oxide	1000	18	19.3	1.2
Molybdenum Oxide	700	56	8.9	8.4
Tungsten Oxide	1600	26	8.3	4.2

^a470 ppm NO in N₂; 100 cm³/min flow

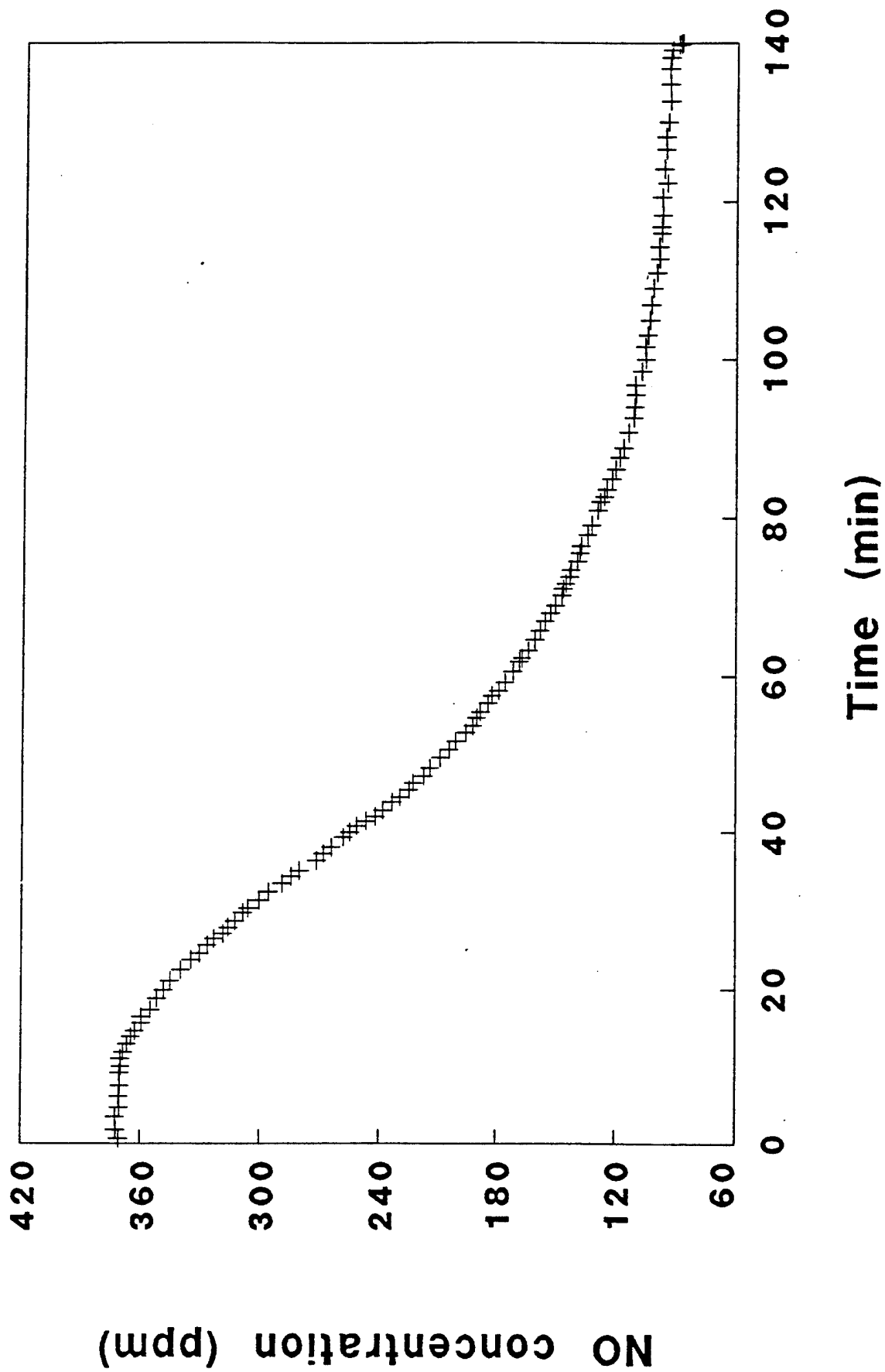


Figure 14. Time Profile of NO Decomposition on Solid Electrolyte

TABLE 3. SELECTIVITY TESTS - NO REMOVAL TESTS^a WITH ELECTROCATALYSTS AND ENHANCED SURFACE AREA ELECTROLYTES IN THE PRESENCE OF OXYGEN

Electrocatalyst Type	Firing Temperature °C	Percentage NO Removal @ 0.3% O ₂	Percentage NO Removal @ 1% O ₂	Percentage NO Removal @ 2% O ₂
Proprietary Group 8 Metal Oxide	700	45 ^b	0	-
Proprietary Group 8 Metal Oxide	800	4 ^c	0	0
Proprietary Group 8 Metal Oxide	900	0	-	-
Iron Oxide	700	0	-	-
Iron Oxide	800	0	0	-
Iron Oxide	1000	-	0	-
Vanadium Oxide	700	-	-	-
Vanadium Oxide	1000	-	0	-
Molybdenum Oxide	700	-	0	-
Tungsten Oxide	1600	-	-	4 ^d

^a100 cm³/min flow

^bCurrent density = 11.2 mA/cm² ; Current efficiency = 5.3%

^cCurrent density = 6.9 mA/cm² ; Current efficiency = 0.8%

^dCurrent density = 8.3 mA/cm² ; Current efficiency = 0.6%

2. High-Temperature Runs

High-temperature tests were run with 1.5-inch diameter, 1/16-inch thick, yttria-stabilized zirconia (YSZ) disks and YSZ honeycomb with various electrocatalysts. Electrocatalysts were prepared and applied to the electrolyte by IGR Enterprises using proprietary techniques. The electrocatalysts tested were mainly transition metal oxides. Tests were performed to determine the effect of electrocatalysts on NO_x reduction and selectivity. Preliminary testing, performed using only electrical data, indicated that higher NO activities were achieved with electrocatalysts than without electrocatalysts. Table 4 shows that up to 29 times higher NO current could be achieved with a tungsten electrocatalyst than without. Limited disk tests were run using the NDIR analyzer. Table 5 shows the results of NO reduction tests in oxygen-free gas.

More-extensive testing was performed using YSZ honeycomb. Tests were performed in the presence of various concentrations of oxygen. Table 6 shows the NO removal percentages for YSZ honeycomb at oxygen concentrations from 2 percent to 8 percent. Even in the presence of oxygen, up to 69.7 percent NO reduction was achieved with the high-temperature zirconia-electrocatalyst system. In general, increasing oxygen concentration corresponded to lower NO reduction.

D. Spread Sheet Analysis

A system analysis was performed using a spread-sheet-based computer program to determine the size, pressure drop, and electricity consumption for various electrochemical NO_x emission control systems.

1. Assumptions

Operating conditions for a jet engine test were found with a preliminary literature search. A large range of temperature, exhaust flow, and NO_x flow conditions was found and depended upon the operating conditions of the engine (percent power applied) and the type of engine tested. (References 10,11,12) Based on these findings, two different operating conditions were assumed, low and high power. Low-power conditions were: 500°C, 200,000 lb/hr total exhaust flow rate, and 2 lb NO/hr NO_x flow rate. High-power conditions were: 1000°C, 900,000 lb/hr total exhaust flow rate, and 90 lb NO/hr NO_x flow rate.

The NO_x removal system requirements assumed were: 90 percent removal of NO_x, total system pressure drop less than 2 inches of water, and limited amount of space. The area available for the NO_x removal system depends on the type of test facility being used. Two types of facilities were observed at Tyndall Air Force Base. The first required the removal of the engine from the plane. This type had a limit of approximately 71 square feet (9 feet 6 inches in diameter) cross-sectional area for exhaust gas flow. Figure 15 shows a schematic of the test cell with an electrochemical NO_x removal system in place. The second type was capable of testing the engines

TABLE 4. NO REDUCTION ACTIVITY - NO REDUCTION TESTS^a
USING HIGH-TEMPERATURE DISKS IN THE
ABSENCE OF OXYGEN

Electrocatalyst	870°C A(NO) ^b	970°C A(NO)	1070°C A(NO)
Baseline YSZ	1.0	1.0	1.0
Molybdenum Oxide	5.2	21.9	-
Tungsten Oxide	2.9	29.0	16.1
Tungsten Oxide	5.1	22.6	28.7
High Surface YSZ	1.4	3.2	2.4
Nickel Oxide	3.9	16.8	19.0
Vanadium Oxide	3.9	21.3	17.7

^a100 cm³/min flow

$${}^b A(\text{NO}) = \frac{\text{mA @ 1.0V w/ 3\% NO in He w/ Electrocatalyst}}{\text{mA @ 1.0V w/ 3\% NO in He - Baseline YSZ}}$$

TABLE 5. HIGH-TEMPERATURE DISK RUNS - NO REMOVAL
TESTS^a WITH ELECTROCATALYSTS IN THE ABSENCE
OF OXYGEN

Electrocatalyst	Temperature °C	Initial Conc NO (ppm)	Percent NO Removal
Vanadium Oxide	970	270	44.4
Vanadium Oxide	970	435	59.8
Tungsten Oxide	870	430	28.6
Tungsten Oxide	970	430	11.6

^a100 cm³/min flow; Applied Voltage = 2.0 V

TABLE 6. HIGH-TEMPERATURE HONEYCOMB RUNS - NO REMOVAL TESTS WITH ELECTROCATALYSTS IN THE PRESENCE OF OXYGEN

Electro-catalyst ^a	Oxygen Conc (%)	Temp °C	Initial NO Conc (ppm)	Percent NO Removal	Current Density (mA/cm ²)	Applied Voltage (V)
Molybdenum ^b	2	970	400	35.0	2.86	0.55
Molybdenum ^b	4	970	408	17.6	2.86	0.45
Molybdenum ^b	2	970	77	23.4	2.86	0.47
Tungsten ^b	2	800	370	26.5	1.71	1.30
Tungsten ^b	4	800	360	20.8	2.29	1.30
Tungsten ^b	8	800	335	13.4	2.86	1.25
Tungsten ^b	2	800	85	52.9	2.57	1.30
Tungsten ^c	6	800	340	32.4	2.00	1.30
Tungsten ^c	2	970	380	69.7	2.86	0.90
Tungsten ^c	4	970	373	54.4	2.86	0.90
Tungsten ^c	8	970	265	35.8	2.86	0.60

^aAll electrocatalysts are metal oxides

^bFlow = 100 cm³/min

^cFlow = 35 cm³/min

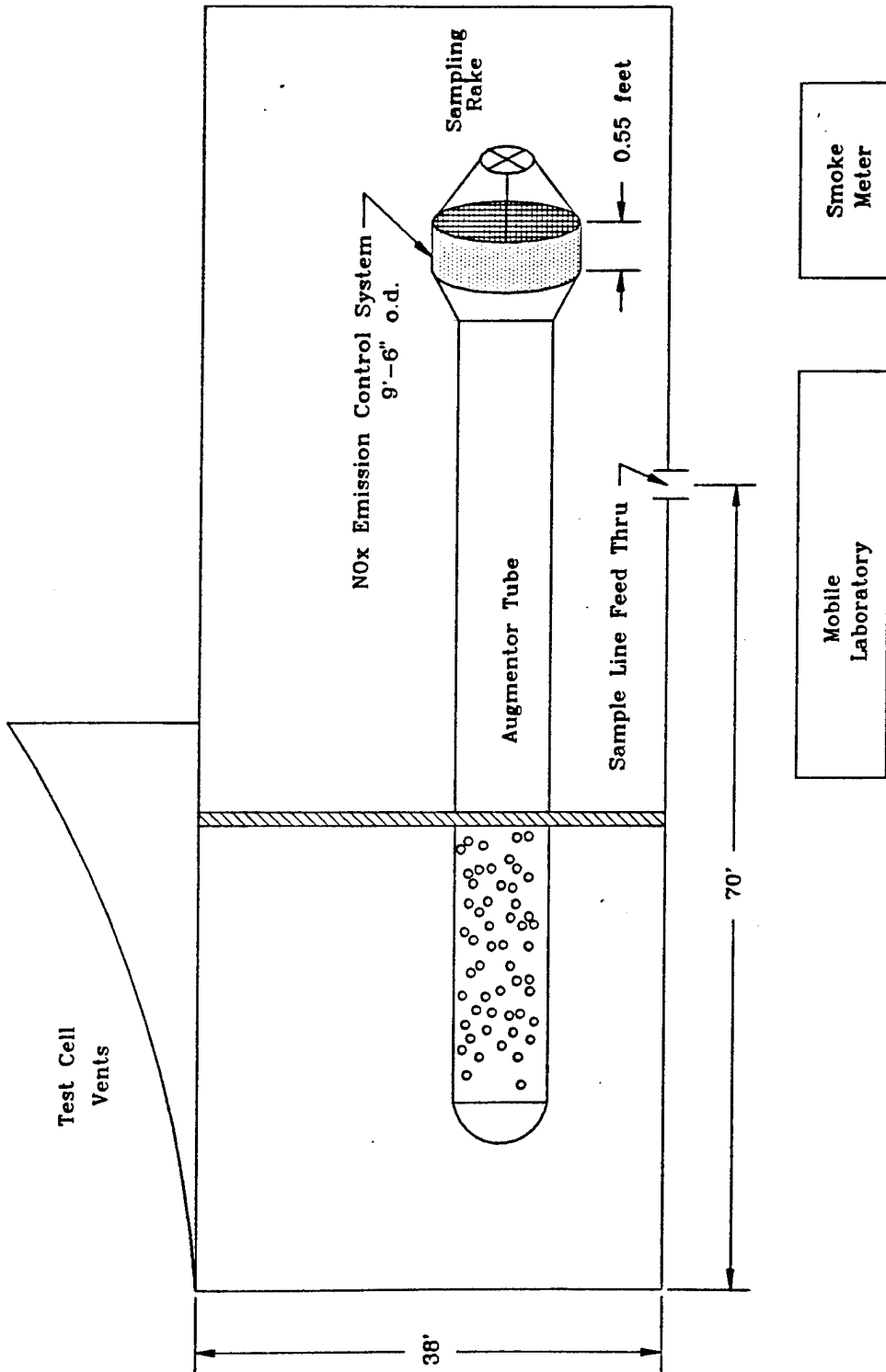


Figure 15. Schematic of Test Cell 8

either in the plane or out. This type had a cross-sectional area of approximately 175 square feet (15-foot diameter). The 71-square-foot unit was used as the basis for the calculations in this report.

In general, experimental electrolyte electrical data (current density and applied voltage) were used whenever possible. Present experiments showed limited, but improving, selectivity to NO over oxygen and thus low current efficiencies. For these calculations, the best conditions for an optimum electrochemical cell are assumed (high current density at low voltages and 100 percent current efficiencies) for a number of calculations. High current densities at low voltages with high current efficiencies are expected in commercial applications with further electrocatalyst development work.

Other assumptions include:

- o a honeycomb-type electrolyte with 0.02-inch-thick electrolyte will be used
- o the exhaust gas density and viscosity is the same as air at the given temperature
- o all NO_x is assumed to be in the form of NO

2. Equations

Three basic equations were used for the spread sheet calculations: pressure drop, minimum electrolyte surface area required, and actual width and height of the reactor.

a. Pressure Drop

Pressure drop correlations were taken from Perry's "Chemical Engineers' Handbook" (page 5-26) for isothermal flow in a horizontal duct. (Reference 13)

$$\text{Pressure Drop} = fLG^2 / 2g_c R_H(\rho)$$

where,

- f = Fanning friction factor = function of Reynolds number
- L = gas path length
- G = mass velocity = velocity x density
- $g_c = 32.17 \text{ lb ft}/(\text{lb force})(\text{sec}^2)$
- $R_H = \text{hydraulic radius} = \text{side}/4$ for a square channel
- $\rho = \text{density}$

First, the channel size for the honeycomb, reactor width, and number of cells in the stack are chosen and, for the operating temperature assumed, the linear gas flow velocity (V in ft/s) is calculated. The temperature also sets the fluid viscosity

(μ in lb/ft-s) and density (ρ in lb/ft³). From these variables, the Reynolds number can be calculated by:

$$\text{Reynolds Number (Re)} = (2 R_H)(V)(\rho)/(\mu)$$

The Reynolds number is a measure of the turbulence in the gas flow, which affects the pressure drop in the Fanning friction factor, f . For laminar flow ($\text{Re} < 2100$), the correlation,

$$f = 16/\text{Re},$$

is used. For $2100 < \text{Re} < 100,000$, the correlation, (Reference 14)

$$f = 0.0791/\text{Re}^{1/4},$$

is used. For $\text{Re} > 100,000$, the correlation, (Reference 15)

$$f = (1/(4.0 \log_{10}(2R_H/0.000005) + 2.28))^{1/2},$$

is used. Gas path length is determined from the reactor width, number of cells in the stack, and from the minimum electrolyte surface area calculation:

$$L = \text{Area}/[(\# \text{ of cells})/\text{width}]$$

Once the gas path length and the friction factor are determined, the pressure drop can be calculated.

b. Minimum Electrolyte Surface Area

After an operating temperature is assumed, the electrical properties of the electrolyte are used to calculate the minimum electrolyte surface area required to decompose 90 percent of the NO_x. The basic equation used is

$$\text{Minimum Surface Area} = (\text{Current Required})/(\text{Current Density})$$

The required current for the removal of NO_x can be calculated from a form of Faraday's Law:

$$\text{Current Required} = (N_{eq})(F)(\text{gmoles NO}_x \text{ removed/s})/(\text{current eff})$$

where,

N_{eq} = number of electrons/molecule NO_x reacted;

=2 for each O atom in reaction

F = Faraday's Constant = 96,489 coulomb/ N_{eq}

gmoles NO_x removed/sec calculated from NO Flow (lb/hr)

current eff = current efficiency, assumed to be 100 percent
in most cases

The minimum surface area determines the amount of electrolyte required, thus fixing the capital cost of the equipment.

c. Actual Width and Height of Reactor and Equivalent Reactor Diameter

Honeycomb is assumed to have open channels separated by 0.02-inch ceramic support members (see Figure 16). Thus the actual cell width is the active reactor width (where reaction takes place) plus the width of supporting members of the honeycomb.

Actual Cell Width = (Reactor Width)(Channel Size + 0.02)/Channel Size

Reactor Width is defined as the Active Reactor Width where decomposition of NO_x occurs.

The actual reactor height is the sum of the open channels plus the electrolyte layers:

Actual Reactor Height = (# of Cells)(Channel Size + 0.02)

The actual height and width, along with the gas path length, determine the volume of the NO_x emission control reactor. This can be compared to the allowable reactor size for a given jet engine test cell.

The equivalent reactor diameter is found by assuming that the cross sectional area to flow equals the actual reactor width times the actual reactor height. By assuming this area has circular geometry, the equivalent diameter can be calculated.

3. Results

The spread sheet requires the input of temperature (500°C or 1000°C), channel size, number of cells, and reactor width. The spread sheet calculates the height, width, and equivalent diameter of the reactor, and the pressure drop through the reactor. Also calculated are overall voltage and current required per cell.

Initial spread sheet runs used data generated under DOE METC and PETC prior to the start of this program. The electrolyte used under PETC was a stabilized ceria operating at 500°C which achieved a current density of 22.7 mA/cm² at 1.5 V. The METC electrolyte was a stabilized zirconia operating at temperatures up to 1000°C at a current density of 137.1 mA/cm² at 0.45 V. Initially, all current was assumed to decompose NO_x (current efficiency = 100 percent). Runs were performed to determine the effect of changing channel size, reactor width, reactor length, and number of cells on pressure drop and reactor diameter. The analysis also determined which configuration (high-temperature or low-temperature) is limiting and therefore most greatly effects design.

Table 7 shows calculated changes in pressure drop and reactor diameter with variations in honeycomb channel size for the 500°C and 1000°C cases. In both cases the minimum electrolyte surface area is specified. The number of cells (230) and reactor width (8.5 feet) is also set. In both cases, the pressure drop decreases with increasing channel size and the reactor diameter

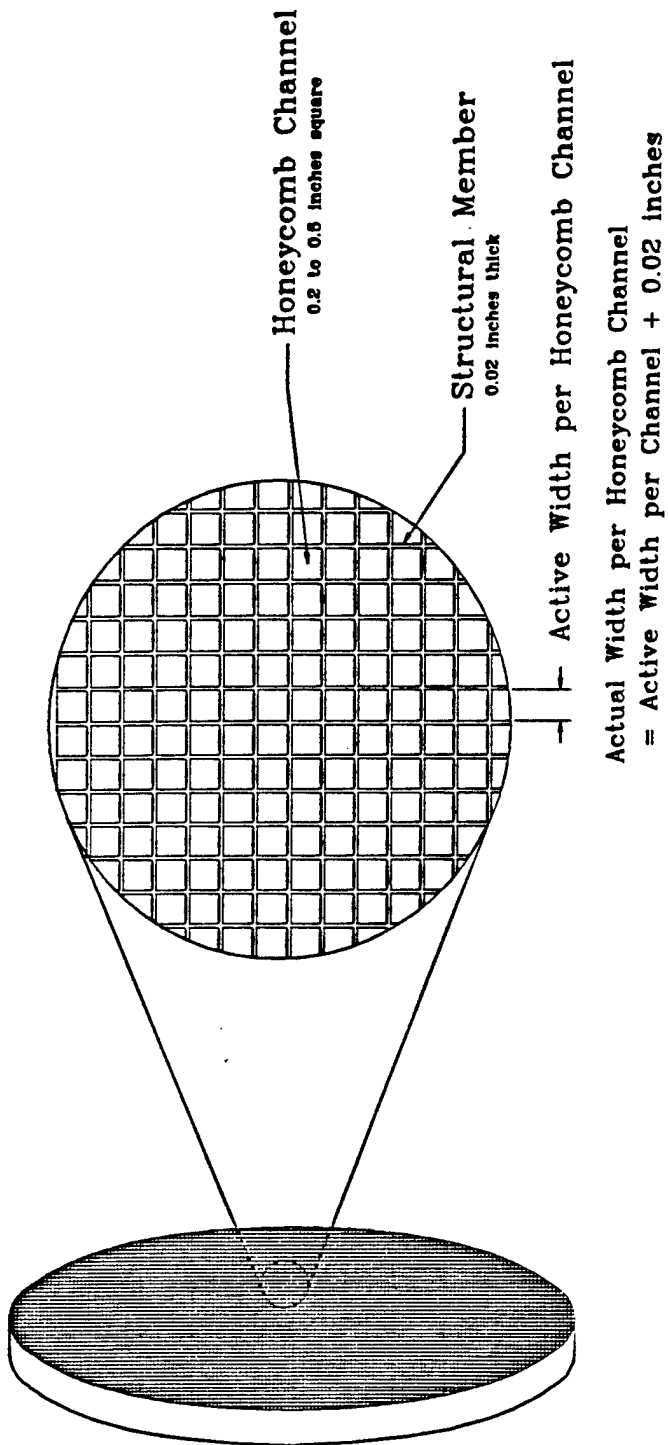


Figure 16. Honeycomb Channel Diagram

increases. The results indicate the pressure drop is not a problem with the low-temperature case, and that only reactor diameter is limiting. High-temperature operation indicates the channel size must be below about 0.4 inches to maintain a reasonable reactor diameter but must be above approximately 0.25 inches to keep the pressure drop below three inches of water.

In Table 8, the channel width is varied between 0.25 and 0.45 inches for an 8-foot wide reactor. Again pressure drop is not a problem in the low-temperature case. Thus the high-temperature reactor is limiting and the high-temperature reactor sizing must be checked for the low-temperature case. Table 9 shows the pressure drop for the low-temperature case with the high-temperature reactor sizing (0.28 foot long). The longer reactor increases the pressure drop, but the values are within the specified limits. Also the electrolyte surface area required is approximately five times the minimum required, thus NOx removal will be greatly enhanced.

Table 10 shows the effect of varying the number of cells and the reactor width. Increasing the number of cells (increasing the reactor height) allows the reactor length to be decreased, thereby decreasing pressure drop. But increasing the number of cells also increases the reactor diameter. The same effect occurs when the reactor width is increased.

In Table 11, the channel size (0.35 inches), the number of cells (272), and the reactor width (8.00 feet) are chosen to give an approximately square reactor (8.46 feet by 8.39 feet), which corresponds to a reactor diameter of 9.5 feet. The reactor length is then varied to achieve the maximum allowable pressure drop (approximately three inches of water). A reactor length of 0.72 feet gives a pressure drop of about three inches of water with an electrolyte surface area above the minimum requirement of 1,044 feet² (about twice the minimum required surface area).

Table 12 shows the effect of reduced current efficiency on reactor performance (minimum required electrolyte surface area). As current efficiency decreases, the electrolyte surface area required to remove 90 percent of the NOx increases. The reactor specified in Table 12 (0.35-inch channels, 9.5 foot reactor diameter, 0.719 feet long) can remove 90 percent of NOx if the current efficiency is above about 33 percent. Low current efficiencies also increase operating costs because current is lost to oxygen pumping and other parasitic sources.

Presently, the highest experimental current efficiency obtained is 31.0 percent at a current density of 2.0 mA/cm² for yttria stabilized ceria electrolyte material with the proprietary group 8 electrocatalyst coating operated at 500°C. This electrolyte/electrocatalyst system cannot be made into a 9.5-foot diameter unit without exceeding the pressure drop and reactor size limits in both the 15-foot diameter test cell and the 9.5-foot test cell.

TABLE 7. EFFECT OF CHANGES IN HONEYCOMB CHANNEL SIZE

T	Channel Size	# of Cells	Reactor Width	Reactor Length	Area Above Minimum	Pressure Drop	Gas Velocity	Actual Width	Actual Height	Reactor Diameter	Current Density	Total Voltage	Min Electrolyte Surface Area	Power Required	Current Efficiency	Current/Cell
G.	Inches		ft	ft	sq ft	Inches H ₂ O	ft/s	ft	ft	ft	mA/sq cm	Volts	sq ft	kW	%	Amps
500	0.1	200	8.50	0.04	0	0.27	116.25	10.20	2.30	5.47	22.70	345	73	2.30	100	6.67
500	0.15	200	8.50	0.04	0	0.08	77.50	9.63	3.28	6.32	22.70	345	73	2.30	100	6.67
500	0.2	200	8.50	0.04	0	0.03	58.13	9.35	4.22	7.09	22.70	345	73	2.30	100	6.67
500	0.25	200	8.50	0.04	0	0.02	46.50	9.18	5.18	7.76	22.70	345	73	2.30	100	6.67
500	0.3	200	8.50	0.04	0	0.01	38.75	9.07	6.13	8.41	22.70	345	73	2.30	100	6.67
500	0.35	200	8.50	0.04	0	0.01	33.21	8.99	7.09	9.01	22.70	345	73	2.30	100	6.67
500	0.4	200	8.50	0.04	0	0.00	29.08	8.93	8.05	9.56	22.70	345	73	2.30	100	6.67
500	0.45	200	8.50	0.04	0	0.00	25.83	8.88	9.01	10.09	22.70	345	73	2.30	100	6.67
500	0.5	200	8.50	0.04	0	0.00	23.25	8.84	9.97	10.59	22.70	345	73	2.30	100	6.67
1000	0.1	200	8.50	0.28	0	57.01	683.67	10.20	2.30	5.47	137.10	103.5	516	29.57	100	285.69
1000	0.15	200	8.50	0.28	0	16.89	655.76	9.63	3.28	6.32	137.10	103.5	516	29.57	100	285.69
1000	0.2	200	8.50	0.28	0	7.13	491.64	9.35	4.22	7.09	137.10	103.5	516	29.57	100	285.69
1000	0.25	200	8.50	0.28	0	3.85	393.47	9.18	5.18	7.76	137.10	103.5	516	29.57	100	285.69
1000	0.3	200	8.50	0.28	0	2.11	327.89	9.07	6.13	8.41	137.10	103.5	516	29.57	100	285.69
1000	0.35	200	8.50	0.28	0	1.33	281.05	8.99	7.09	9.01	137.10	103.5	516	29.57	100	285.69
1000	0.4	200	8.50	0.28	0	0.88	245.92	8.93	8.05	9.56	137.10	103.5	516	29.57	100	285.69
1000	0.45	200	8.50	0.28	0	0.63	218.56	8.88	9.01	10.09	137.10	103.5	516	29.57	100	285.69
1000	0.5	200	8.50	0.28	0	0.48	198.73	8.84	9.97	10.59	137.10	103.5	516	29.57	100	285.69

TABLE 8. EFFECT OF CHANGES IN HONEYCOMB CHANNEL SIZE (8-FT-WIDE REACTOR)

T	Channel Size	# of Cells	Reactor Width	Reactor Length	Area Above Minimum	Pressure Drop	Gas Velocity	Actual Width	Actual Height	Reactor Diameter	Current Density	Total Voltage	Min Electrolyte Surface Area	Power Required	Current Efficiency	Current/Cell
G.	Inches		ft	ft	sq ft	Inches H ₂ O	ft/s	ft	ft	ft	mA/sq cm	Volts	sq ft	kW	%	Amps
500	0.25	200	8.00	0.04	0	0.02	49.41	8.64	5.18	7.55	22.70	345	73	2.30	100	6.67
500	0.3	200	8.00	0.04	0	0.01	41.17	8.53	6.13	8.16	22.70	345	73	2.30	100	6.67
500	0.35	200	8.00	0.04	0	0.01	35.29	8.46	7.09	8.74	22.70	345	73	2.30	100	6.67
500	0.4	200	8.00	0.04	0	0.00	30.98	8.40	8.05	9.28	22.70	345	73	2.30	100	6.67
500	0.45	200	8.00	0.04	0	0.00	27.45	8.36	9.01	9.79	22.70	345	73	2.30	100	6.67
1000	0.25	200	8.00	0.28	0	4.31	418.06	8.64	5.18	7.55	137.10	103.5	516	29.57	100	285.69
1000	0.3	200	8.00	0.28	0	2.48	348.36	8.53	6.13	8.16	137.10	103.5	516	29.57	100	285.69
1000	0.35	200	8.00	0.28	0	1.57	298.61	8.46	7.09	8.74	137.10	103.5	516	29.57	100	285.69
1000	0.4	200	8.00	0.28	0	1.05	261.29	8.40	8.05	9.28	137.10	103.5	516	29.57	100	285.69
1000	0.45	200	8.00	0.28	0	0.74	232.26	8.36	9.01	9.79	137.10	103.5	516	29.57	100	285.69

TABLE 9. EFFECT OF CHANGES IN REACTOR LENGTH ON 500°C REACTOR

T	Channel Size	# of Cells	Reactor Width	Reactor Length	Area Above Minimum	Pressure Drop	Gas Velocity	Actual Width	Actual Height	Reactor Diameter	Current Density	Total Voltage	Min Electrolyte Surface Area	Power Required	Current Efficiency	Current/Cell
C	Inches		ft	ft	sq ft	Inches H ₂ O	ft/s	ft	ft	ft	mA/sq cm	Volts	sq ft	W	%	Ampe
1000	0.25	230	8.00	0.28	0	4.31	418.08	8.64	5.18	7.55	137.10	103.5	516	29.57	100	285.69
1000	0.3	230	8.00	0.28	0	2.49	348.38	8.53	6.13	6.16	137.10	103.5	516	29.57	100	285.69
1000	0.35	230	8.00	0.28	0	1.57	298.61	8.46	7.09	6.74	137.10	103.5	516	29.57	100	285.69
1000	0.4	230	8.00	0.28	0	1.05	261.28	8.40	8.05	6.28	137.10	103.5	516	29.57	100	285.69
1000	0.45	230	8.00	0.28	0	0.74	232.28	8.38	9.01	6.79	137.10	103.5	516	29.57	100	285.69
500	0.25	230	8.00	0.28	442	0.14	49.41	8.64	5.18	7.55	22.70	345	73	2.30	100	6.97
500	0.3	230	8.00	0.28	442	0.06	41.17	8.53	6.13	6.16	22.70	345	73	2.30	100	6.97
500	0.35	230	8.00	0.28	442	0.05	35.29	8.46	7.09	6.74	22.70	345	73	2.30	100	6.97
500	0.4	230	8.00	0.28	442	0.03	30.88	8.40	8.05	6.28	22.70	345	73	2.30	100	6.97
500	0.45	230	8.00	0.28	442	0.02	27.45	8.38	9.01	6.79	22.70	345	73	2.30	100	6.97

TABLE 10. EFFECT OF CHANGES IN NUMBER OF CELLS AND REACTOR WIDTH ON 1000°C REACTOR

T	Channel Size	# of Cells	Reactor Width	Reactor Length	Area Above Minimum	Pressure Drop	Gas Velocity	Actual Width	Actual Height	Reactor Diameter	Current Density	Total Voltage	Min Electrolyte Surface Area	Power Required	Current Efficiency	Current/Cell
C	Inches		ft	ft	sq ft	Inches H ₂ O	ft/s	ft	ft	ft	mA/sq cm	Volts	sq ft	W	%	Ampe
1000	0.25	200	8.00	0.32	0	2.31	343.41	8.46	6.17	6.15	137.10	90	516	29.57	100	326.55
1000	0.35	215	8.00	0.30	0	1.89	319.45	8.46	6.63	6.45	137.10	98.75	516	29.57	100	305.62
1000	0.36	230	8.00	0.28	0	1.57	298.61	8.46	7.09	6.74	137.10	103.5	516	29.57	100	285.69
1000	0.35	245	8.00	0.26	0	1.32	260.33	8.46	7.55	6.02	137.10	110.25	516	29.57	100	268.20
1000	0.35	260	8.00	0.25	0	1.12	264.16	8.46	8.02	6.29	137.10	117	516	29.57	100	252.73
1000	0.35	275	8.00	0.23	0	0.98	249.75	8.46	8.48	6.56	137.10	123.75	516	29.57	100	238.94
1000	0.36	290	8.00	0.22	0	0.83	236.83	8.46	8.94	6.81	137.10	130.5	516	29.57	100	226.58
1000	0.35	230	7.00	0.32	0	2.27	341.27	7.40	7.09	6.17	137.10	103.5	516	29.57	100	285.69
1000	0.35	230	7.50	0.30	0	1.68	316.52	7.83	7.09	6.46	137.10	103.5	516	29.57	100	285.69
1000	0.36	230	8.00	0.28	0	1.57	298.61	8.46	7.09	6.74	137.10	103.5	516	29.57	100	285.69
1000	0.35	230	8.50	0.26	0	1.33	261.05	8.98	7.09	6.01	137.10	103.5	516	29.57	100	285.69
1000	0.35	230	9.00	0.25	0	1.14	265.44	9.51	7.09	6.27	137.10	103.5	516	29.57	100	285.69
1000	0.35	230	9.50	0.24	0	0.98	251.46	10.04	7.09	6.52	137.10	103.5	516	29.57	100	285.69

TABLE 11. EFFECT OF CHANGES IN REACTOR LENGTH ON PRESSURE DROP IN 1000°C REACTOR

T	Channel Size	# of Cells	Reactor Width	Reactor Length	Area Above Minimum	Pressure Drop	Gas Velocity	Actual Width	Actual Height	Reactor Diameter	Current Density	Total Voltage	Min Electrolyte Surface Area	Power Required	Current Efficiency	Current/Cell
C.	Inches		ft	ft	sq ft	Inches H ₂ O	ft/s	ft	ft	ft	mA/sq cm	Volts	sq ft	kW	%	Amps
1000	0.35	272	8.00	0.24	0	0.99	252.50	8.48	8.39	9.50	137.10	122.4	516	29.57	100	241.58
1000	0.35	272	8.00	0.32	174	1.32	252.50	8.48	8.39	9.50	137.10	122.4	516	29.57	100	241.58
1000	0.36	272	8.00	0.40	348	1.66	252.50	8.48	8.39	9.50	137.10	122.4	516	29.57	100	241.58
1000	0.35	272	8.00	0.48	522	1.99	252.50	8.48	8.39	9.50	137.10	122.4	516	29.57	100	241.58
1000	0.35	272	8.00	0.56	696	2.33	252.50	8.48	8.39	9.50	137.10	122.4	516	29.57	100	241.58
1000	0.35	272	8.00	0.64	870	2.66	252.50	8.48	8.39	9.50	137.10	122.4	516	29.57	100	241.58
1000	0.36	272	8.00	0.72	1,044	3.00	252.50	8.48	8.39	9.50	137.10	122.4	516	29.57	100	241.58
1000	0.35	272	8.00	0.80	1,218	3.33	252.50	8.48	8.39	9.50	137.10	122.4	516	29.57	100	241.58

TABLE 12. EFFECT OF CHANGES IN CURRENT EFFICIENCY ON MINIMUM ELECTROLYTE SURFACE AREA IN 1000°C REACTOR

T	Channel Size	# of Cells	Reactor Width	Reactor Length	Area Above Minimum	Pressure Drop	Gas Velocity	Actual Width	Actual Height	Reactor Diameter	Current Density	Total Voltage	Min Electrolyte Surface Area	Power Required	Current Efficiency	Current/Cell
C.	Inches		ft	ft	sq ft	Inches H ₂ O	ft/s	ft	ft	ft	mA/sq cm	Volts	sq ft	kW	%	Amps
1000	0.35	272	8.00	0.719	1,049	3.00	252.50	8.48	8.39	9.50	137.10	122.4	516	29.57	100	241.58
1000	0.35	272	8.00	0.719	958	3.00	252.50	8.48	8.39	9.50	137.10	122.4	607	34.79	85	204.21
1000	0.36	272	8.00	0.719	828	3.00	252.50	8.48	8.39	9.50	137.10	122.4	737	42.24	70	345.11
1000	0.35	272	8.00	0.719	627	3.00	252.50	8.48	8.39	9.50	137.10	122.4	938	53.78	65	430.23
1000	0.35	272	8.00	0.719	275	3.00	252.50	8.48	8.39	9.50	137.10	122.4	1290	73.92	40	603.94
1000	0.35	272	8.00	0.719	1	3.00	252.50	8.48	8.39	9.50	137.10	122.4	1563	98.60	33	732.05
1000	0.36	272	8.00	0.719	(489)	3.00	252.50	8.48	8.39	9.50	137.10	122.4	2004	118.28	25	968.31
1000	0.35	272	8.00	0.719	(3,564)	3.00	252.50	8.48	8.39	9.50	137.10	122.4	5159	265.99	10	2415.77

E. Preliminary Sizing and Economics

As the spread sheet analysis indicates, further technical advances must be made for a true sizing and economic analysis to be prepared. If the reactor assumed in Table 12 (0.35-inch channels, 9.5-foot reactor diameter, 0.719 feet long) is viable preliminary costs can be determined. In the example of Table 12, a total reactor volume of 51 cubic feet is required. Assuming a manufactured cost of \$0.25/cubic inch (verbal quote from Hi Tech Ceramics, Alfred, New York), the electrolyte cost is approximately \$22,000; installed costs, including electrical connections, approximately equal the electrolyte cost, the total cost being approximately \$44,000.

Operating costs can be calculated from the reactor power requirement. For the best case (100 percent current efficiency), the power required to operate the system is 29.57 kilowatts. If we assume 350 days operation, 8 hours per day, at electrical costs of \$0.10/kWhr the operating cost is approximately \$8,300 per year. At the pressure drop break even point (33 percent current efficiency), the operating costs triple to approximately \$25,100 per year.

SECTION III

CONCLUSION AND RECOMMENDATIONS

A. CONCLUSIONS

Proof-of-principle experiments have established the feasibility of electrochemical NOx reduction using solid-state, solid-oxide electrochemical technology. Present data indicate that improvements must be made to increase current efficiency (increases NOx selectivity) at high current densities. Present experiments indicate that high-surface-area electrolytes with transition metal oxide electrocatalysts show promise. Further experiments need to establish space times for better reactor designs.

Spread sheet analysis indicates that reasonable systems can be designed to fit the 9.5-foot diameter jet engine test cell at less than three inches of water pressure drop. Reasonable assumptions for future systems were made (50 percent to 100 percent current efficiencies, 90 percent NOx removal at current densities achieved in preliminary experiments) and viable systems were possible. These systems can handle temperatures from 500°C to 1000°C. Improved data are required better to determine sizes and pressure drops for actual systems.

B. RECOMMENDATIONS

Further laboratory-scale work is required for development of electrolyte and electrocatalyst, and for surface area enhancement. In particular, improvements are needed to enhance current efficiencies at high current densities. Once viable electrochemical characteristics are established, ceramic mechanical properties and cell designs should be developed.

This technology looks promising for jet engine test cell applications if the technical goals can be more closely approached (especially higher current efficiency). Once testing continues with larger flow through (honeycomb) systems, actual gas streams can be tested. Other concerns to be considered are cell longevity and vibration effects.

SECTION IV

REFERENCES

1. Urban, Charles, Evaluation of NOx Reduction Technology for Natural Gas Industry Prime Movers, GAS RESEARCH INSTITUTE Special Report, Contract Number 5084-251-1101, Chicago, pp. 10-16, August 1987.
2. Cook, W.J., Siwajek, L., Neyman, M., and Gordon, A., NOx Abatement in Natural Gas Combustion Exhaust Gases by Solid-State Electrochemical Technology, GAS RESEARCH INSTITUTE Topical Report, Contract Number 5084-251-1101, Chicago, September 1987.
3. Seinfeld, J.H., Atmospheric Chemistry and Physics of Air Pollution, John Wiley & Sons, New York, p.81, 1986.
4. Bulletin 542, U.S. Bureau of Mines, p. D-354 CRC, 1954.
5. Polin, G.W. and Eischens, R.P., "Infrared Study of Adsorbed Corrosion Inhibitors: Butyl Nitrate and Nitric Oxide on Iron-Iron Oxide," J. Electrochem. Soc., 113, 216, 1966.
6. Naccache, C. and Ben Taarit, Y., "Nature of Nitric Oxide and Nitrogen Dioxide Adsorbed on Chromium and Nickel Exchanged Zeolites," J. Chem. Soc. Faraday Trans. I, 69, 1475, 1973.
7. Tamura, T. and Hamamura, T., "Coadsorption of Nitric Oxide, Nitrogen, and Oxygen on a Polycrystalline Tungsten Surface," Shinku, 23(9), 425-9, (Japan) 1980.
8. Howe, R.F., and Kemball, C., "Poisoning of a Supported Molybdenum Olefin Disproportionation Catalyst," J. Chem. Soc. Faraday Trans. I, 70, 1153-1161, 1974.
9. Cook, W.J., Hossain, S., Neyman, M., and Gordon, A., Simultaneous Particulates, NOx, SOx Removal from Flue Gas by All Solid-State Electrochemical Technology, Technical Progress Report, U.S. Department of Energy Pittsburgh Energy Technology Center, August 31, 1988.
10. Spicer, C.W., Holdren, M.W., Miller, S.E., Smith, D.L., Smith, R.N., Kuhlman, M.R., and Hughes, D.P., Aircraft Emissions Characterization: TF41-A2, TF30-P103, and TF30-P109 Engines, ESL-TR-87-27, Battelle Columbus Division, Columbus, Ohio, December 1987.
11. Spicer, C.W., Holdren, M.W., Miller, S.E., Smith, D.L., Smith, R.N., and Hughes, D.P., Aircraft Emissions Characterization, ESL-TR-87-63, Battelle Columbus Division, Columbus, Ohio, March 1988.

12. Seitchek, G.D., Aircraft Engine Emissions Estimator, ESL-TR-85-14, Air Force Engineering and Services Center, Tyndall AFB, November 1985.
13. Perry, R.H., and Chilton, C.H., editors, Chemical Engineers' Handbook, Fifth Edition, McGraw-Hill Company, New York, p. 5-26, 1973.
14. Bird, R.B., Stewart, W.E, and Lightfoot, E.N., Transport Phenomena, John Wiley & Sons, New York, p. 187, 1960.
15. Welty, J.R., Wicks, C.E., And Wilson, R.E., Fundamentals of Momentum, Heat, and Mass Transfer, John Wiley & Sons, New York, p. 207, 1976.